Zircon xenocrysts from Easter Island (Rapa Nui) reveal hotspot activity since the middle Jurassic

Yamirka Rojas-Agramonte[1], Natalia Pardo[2], Douwe J.J. van Hinsbergen[3], Christian Winter[4], María Paula Marroquín-Gómez[5], Shoujie Liu[6], Axel Gerdes[7], Richard Albert[7], Shitou Wu[8], and Antonio Garcia-Casco[9]

[1]Christian-Albrechts-Universität zu Kiel
[2]Universidad de Los Andes
[3]Utrecht University
[4]University of Kiel
[5]The University of Arizonauni
[6]Beijing SHRIMP Centre, Chinese Academy of Geological Sciences
[7]Goethe University Frankfurt
[8]State Key Laboratory of Lithospheric Evolution, Institute of Geology and Geophysics, Chinese Academy of Sciences
[9]Universidad de Granada

November 29, 2023

Abstract

The 0–2.5 Ma volcanism in Easter Island (Rapa Nui) emerges just east of the East Pacific Rise on young (Pliocene, 3–4.8 Ma) ocean floor. Here, we report the finding of mantle-derived zircon grains retrieved from Easter Island beach sands and red soils that are much older than the Easter Island volcanism and its underlying lithosphere. A large population of 0–165 Myr old zircons have coherent oxygen (δ18O(zircon) 3.8– 5.9These results are consistent with the crystallization of zircon from plume-related melts. In addition, a chemically diverse population with ages as old as Precambrian was also found. We thus suggest that the Easter hotspot started at least ˜165 Ma ago. A large population of ˜160-164 Ma zircons could signal an intense initial massive melting phase associated with the formation of a Large Igneous Province (LIP) upon the first arrival of the plume. We use plate reconstructions to show that such a LIP would have formed on the Phoenix Plate. It would have subducted below the Antarctic Peninsula around 100-105 Ma, offering a solution for the enigmatic Palmer Land deformation event, previously proposed to result from a collision with an unknown indenter. Our findings show that asthenospheric mantle-derived xenocryst zircon cargo, as recently reported from Galápagos, may not be an exception. The here-reported "ghost" of a prolonged hotspot activity suggests that the Easter hotspot and the sub-lithospheric mantle in which it is entrained remained mantle-stationary for at least 165 Ma.

Hosted file

`979640_0_art_file_11599377_s48pcg.docx` available at https://authorea.com/users/702732/articles/688564-zircon-xenocrysts-from-easter-island-rapa-nui-reveal-hotspot-activity-since-the-middle-jurassic

Hosted file

`979640_0_supp_11599493_s4blgl.docx` available at https://authorea.com/users/702732/articles/

688564-zircon-xenocrysts-from-easter-island-rapa-nui-reveal-hotspot-activity-since-the-middle-jurassic

AGU PUBLICATIONS

AGU Word Manuscript Template

Zircon xenocrysts from Easter Island (Rapa Nui) reveal hotspot activity since the middle Jurassic

Yamirka Rojas-Agramonte[1,2*], Natalia Pardo[3], Douwe J.J. van Hinsbergen[4], Christian Winter[1] María Paula Marroquín-Gómez[5], Shoujie Liu[6], Axel Gerdes[7,8], Richard Albert[7,8], Shitou Wu[9], Antonio García-Casco[10,11*]

[1]Institute of Geosciences, Christian-Albrechts-Universität zu Kiel, Otto-Hahn-Platz 1, 24118 Kiel, Germany
[2]Institute of Geosciences, University of Mainz, 55099 Mainz, Germany
[3]Departamento de Geociencias, Universidad de los Andes, Bogotá, Colombia
[4]Department of Earth Sciences, Utrecht University, Princetonlaan 8a, Utrecht University, 3584 CB Utrecht, The Netherlands
[5]The University of Arizona Department of Geosciences Tucson, Arizona, 85721, EE. UU.
[6]Beijing SHRIMP Centre, Chinese Academy of Geological Sciences, 26 Baiwanzhuang Road, 100037 Beijing, China
[7]Department of Geosciences, Goethe University Frankfurt, Altenhoferallee 1, 60438 Frankfurt am Main, Germany
[8]FIERCE (Frankfurt Isotope and Element Research Center), Goethe University Frankfurt am Main, Germany
[9]State Key Laboratory of Lithospheric Evolution, Institute of Geology and Geophysics, Chinese Academy of Sciences, No. 19, Beitucheng Western Road, Chaoyang District, Beijing, 100029, P.R.China
[10]Department of Mineralogy and Petrology, University of Granada, Fuentenueva s/n, 18071 Granada, Spain
[11]Andalusian Earth Sciences Institute (IACT), University of Granada-CSIC 18100 Armilla, Granada, Spain
Corresponding authors: Yamirka Rojas-Agramonte (Yamirka.rojas@ifg.uni-kiel.de); Antonio Gracía-Casco (agcasco@ugr.es)

Key Points:

- Presence of ~0-165 Myr old zircons with coherent O and εHf(t) mantle isotopic signatures in the Easter plume.

- A large population of ~165 Ma zircons could signal a massive melting phase associated with formation of a Large Igneous Province (LIP)
- This LIP probably subducted below the Antarctic Peninsula around 100-105 Ma likely related to the Palmer Land deformation event.

Abstract

The 0–2.5 Ma volcanism in Easter Island (Rapa Nui) emerges just east of the East Pacific Rise on young (Pliocene, 3–4.8 Ma) ocean floor. Here, we report the finding of mantle-derived zircon grains retrieved from Easter Island beach sands and red soils that are much older than the Easter Island volcanism and its underlying lithosphere. A large population of 0–165 Myr old zircons have coherent oxygen ($\delta_{18}O_{(zircon)}$ 3.8– 5.9‰) and hafnium mantle isotopic signatures ($\varepsilon Hf_{(t)}$ +3.5–+12.5). These results are consistent with the crystallization of zircon from plume-related melts. In addition, a chemically diverse population with ages as old as Precambrian was also found. We thus suggest that the Easter hotspot started at least ~165 Ma ago. A large population of ~160-164 Ma zircons could signal an intense initial massive melting phase associated with the formation of a Large Igneous Province (LIP) upon the first arrival of the plume. We use plate reconstructions to show that such a LIP would have formed on the Phoenix Plate. It would have subducted below the Antarctic Peninsula around 100-105 Ma, offering a solution for the enigmatic Palmer Land deformation event, previously proposed to result from a collision with an unknown indenter. Our findings show that asthenospheric mantle-derived xenocryst zircon cargo, as recently reported from Galápagos, may not be an exception. The here-reported “ghost” of a prolonged hotspot activity suggests that the Easter hotspot and the sub-lithospheric mantle in which it is entrained remained mantle-stationary for at least 165 Ma.

1 Introduction

Plate tectonics theory straightforwardly explains how oceanic lithosphere is subductable and only becomes a few hundred million years old, whereas continental lithosphere is not, and may become billions of years old. Geochronological databases (U-Pb in zircons) derived from continental crust contain age spectra that cover almost all of Earth’s history (e.g. Condie et al., 2009; Domeier et al., 2018; Rodriguez-Corcho et al., 2022; Wu et al., 2023), whereas oceanic crusts tend to only contain zircons in a narrow age spectrum that coincides with the magmatic age of the crust (e.g. Lissenberg et al., 2009; Rioux et al., 2016). In that context, it is puzzling that an increasing body of literature reports zircon populations collected at mid-oceanic ridges and from remote oceanic hotspot volcanoes that are far older than the crust they reside in.

Pilot et al. (1998) was the first to report Paleozoic and older zircons from the Central Atlantic mid-ocean ridge. Since this first finding, diverse populations of Paleozoic and older zircons have also again been collected from the Central Atlantic Ridge and reported from the North Atlantic and South Atlantic ridges (Bea et al., 2020; Bjerga & Pedersen, 2021; Bortnikov et al., 2008; Skublov et al., 2022), and recently from intra-oceanic, remote hotspot islands of Hawai’i (Greenough et al., 2021) and Galápagos (Rojas-Agramonte et al., 2022). These ancient zircons cannot have formed from crystallizing magma at the young mid-ocean ridges, or in the oceanic crust below the hotspot volcanoes, and were consequently interpreted as xenocrysts.

In addition, ancient zircon populations were found with narrow age ranges or coherent chemistry. For instance, ~180 Ma zircons were collected from the Southwest Indian Ridge (Cheng et al., 2016) and a ~0–164 Ma population with coherent chemistry was recently reported from Galápagos (Rojas-Agramonte et al., 2022). That zircon can survive asthenospheric mantle conditions in mafic and ultramafic systems and retain its U-Th-Pb and Lu-Hf isotopic signature was shown in laboratory experiments (Bea et al., 2018; Cambeses et al., 2023). Furthermore, xenocrystic zircons are routinely found in ophiolitic mantle sections (e.g. Aitchison et al., 2022; González-Jiménez et al., 2017; Lian et al., 2020; Moghadam et al., 2022; Portner et al., 2011; Proenza et al., 2018; Xiong et al., 2022), and subducted zircons resurface in arc volcanoes (Gao et al., 2022; Rojas-Agramonte et al., 2017; Rojas-Agramonte et al., 2016). The serendipitous findings of zircons have thus been explained as 'ghosts' (Gianni et al., 2023) of either subducted sedimentary zircons entrained in fossil mantle wedges or detached sub-continental mantle lithosphere that float in the asthenospheric mantle (e.g. Bjerga et al., 2022; Gianni et al., 2023; van Hinsbergen et al., 2020; Pilot et al., 1998) or as magmatic zircons that formed during crystallization of mantle plume-related melts (Rojas-Agramonte et al., 2022). The presence of such features in the sub-lithospheric mantle is consistent with equally fortuitous geochemical findings from Atlantic, Pacific, and Indian mid-ocean ridges (Le Roux et al., 2002; Liu et al., 2022; Richter et al., 2020; Urann et al., 2020; Yang et al., 2021).

The preservation of such ghosts could offer novel possibilities to reconstruct the geological history of the mantle. For instance, the finding of a range of zircons from the Jurassic to the present with coherent plume-like chemistries on the Galápagos led Rojas-Agramonte et al. (2022) to postulate that the Galápagos plume may date back far longer than the oldest magmatic products that are typically ascribed to the plume (the Cretaceous Caribbean Large Igneous Province). This suggests xenocrystic zircons on young hotspot islands may offer insight into a far longer geological history of the sub-lithospheric mantle than is preserved on the present oceanic crust.

In this paper, we report on the zircon cargo that we collected during a reconnaissance study of beach sands and soils from the remote Easter hotspot island, 3800 km west of the South American coast in the Pacific Ocean (Fig. 1). The Plio-Pleistocene Easter volcanic Island is built on Pliocene ocean floor (~3–4.8 Ma; (Bonatti et al., 1977; Hagen et al., 1990; Naar & Hey, 1989; Vezzoli & Acocella, 2009), and the oldest zircon that could have formed during volcanism or the underlying sea floor may thus be ~4 Ma old. The oldest seamounts that formed at this hotspot that are preserved on the modern ocean floor are in the Tuamotu Seamount chain and are 48 Ma old (Bello-González et al., 2018). The hotspot likely started earlier, but older seamounts have disappeared through subduction below South America or Antarctica, and the onset of plume activity is unknown. We will use the age distributions and composition of the zircons obtained from the Easter beaches and soils to evaluate whether xenocrysts are present and discuss the possibilities that xenocrystic zircon cargo may offer a novel source of information on mantle and plume-related geological history.

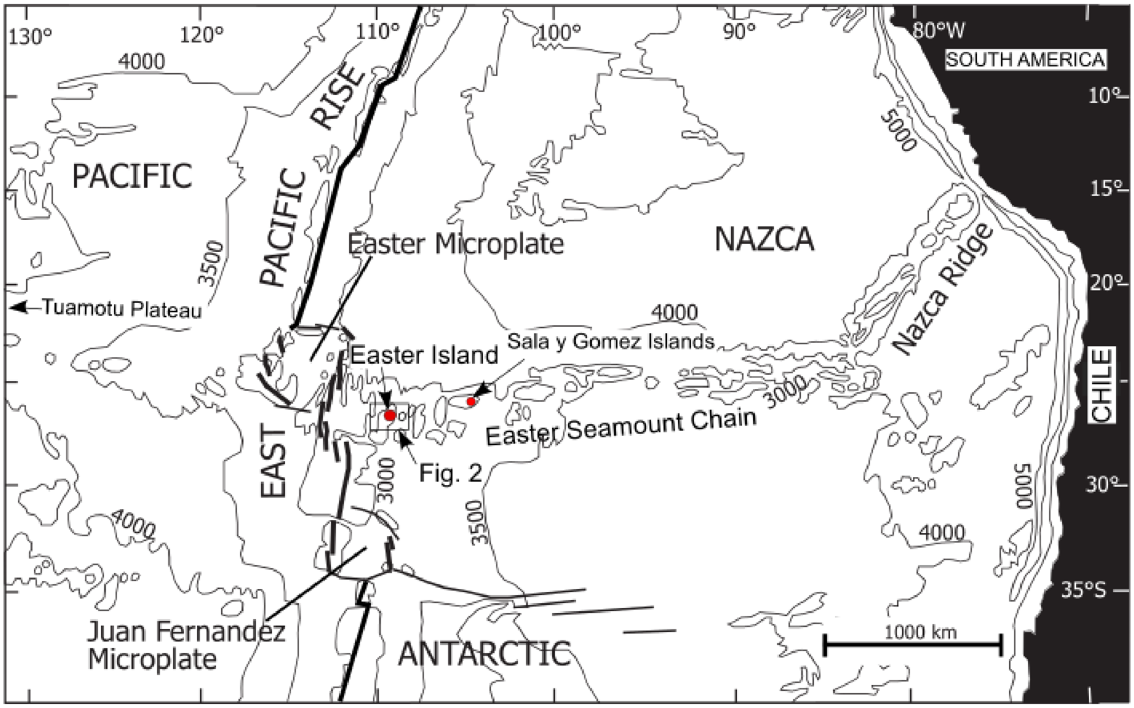

Figure 1. Tectonic realm of the study area showing the location of Easter Island (Rapa Nui) at the westernmost end of the Easter Seamount Chain on the Nazca Plate, east of the East Pacific Rise.

2. Geological background

Easter Island (Rapa Nui, Polynesia) lies on the westernmost edge of the Nazca Plate, close to the East Pacific Rise that forms the spreading ridge with the Pacific Plate (Fig. 1). The Easter hotspot is located above the edge of the Pacific Large Low Shear Velocity Province (LLSVP), and is thought to result from a deep mantle plume that originates at ~2900 km depth near the core-mantle boundary (Burke et al., 2008; Courtillot et al., 2003; Harpp et al., 2014). The youngest seamount chain is located on the Nazca Plate and forms the 2900 km long, E-W trending Easter Seamount Chain with the active Easter-Salas hotspot at its western tip (Bello-González et al., 2018; Ray et al., 2012; Rodrigo et al., 2014; Vezzoli & Acocella, 2009). Eastwards, the Easter Seamount Chain connects to the Nazca Ridge that represents a ~30–20 Ma older portion of the chain (Fig. 1) (Bonatti et al., 1977; Rappaport et al., 1997; Ray et al., 2012; Simons et al., 2002; Stoffers et al., 1994). Between ~48 and 30 Ma, the East Pacific Rise was located just east of the hotspot, and the Tuamotu Seamount chain formed on the Pacific Plate (Bello-González et al., 2018; Hampel, 2002; Rosenbaum et al., 2005). Prior to 48 Ma, the hotspot was presumably located east of the East Pacific Rise (Bello-González et al., 2018; Espurt et al., 2007) (Fig. 1).

The first accounts on the geology and petrography of Easter Island were published by Chubb (1933), Bandy (1937), and Baker (1967), whilst the first comprehensive geological maps were provided by Gonzalez-Ferran & Baker (1974), Gonzales-Ferran et al. (2004), and Gioncada et al. (2010). The island represents the small (160 km^2) emerged portion of three main, coalescing polygenetic shield volcanoes (Poike, Rano, Kau, and Terevaka; Fig. 2), built during the last ~2 Ma on top of a ~3–4.8 Ma old oceanic crust (Fig. 2; Bonatti et al., 1977; Hagen et al., 1990; Naar & Hey, 1989; Vezzoli & Acocella, 2009). The emerged products of these three volcanoes are mainly effusive, strongly affected by marine erosion, and are crosscut by multiple (~100), aligned monogenetic vents (Baker, 1967; Gioncada et al., 2010; Vezzoli & Acocella, 2009). Volcanic products are predominantly basalts, hawaiites, mugearites, and benmoreites, but there are also trachytes and peralkaline rhyolites (Fig. S1; Baker et al., 1974; Bonatti et al., 1977; Boven et al., 1997; Clark & Dymond, 1977; DePaepe & Vergauwen, 1997; Haase et al., 1997). The lavas have a high zirconium content ranging from 137 ppm in the mafic lavas to as high as 1355 ppm in the intermediate and felsic products, which is somewhat not surprising that we have found so many zircons in the detritus of the island (Table S1). Vezzoli & Acocella (2009) identified a general evolution pattern for the island volcanism, starting with a shield stage followed by a non-explosive caldera stage truncating each of the three main edifices, and culminating with the rifting stage of the island, dominated by monogenetic volcanism.

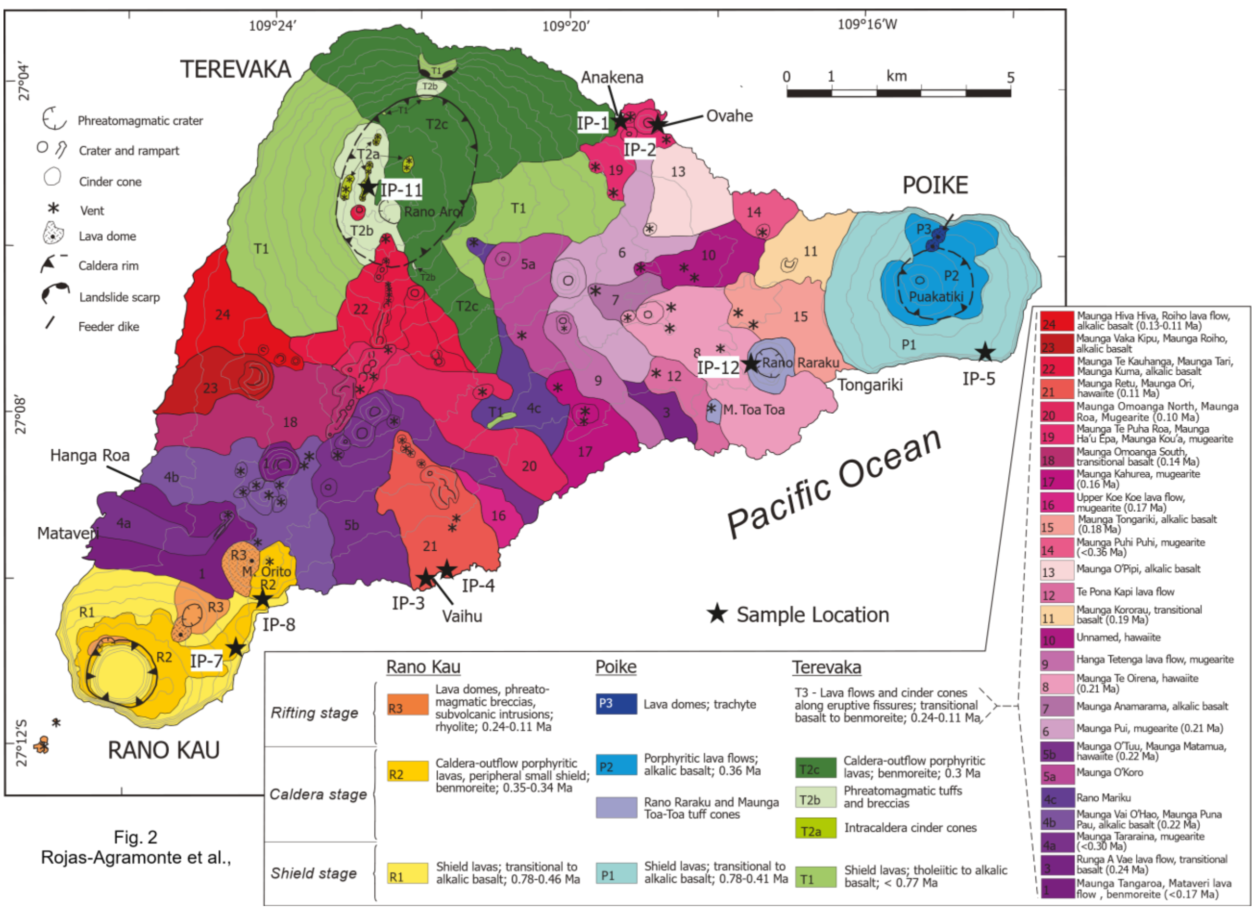

Figure 2. Geological map of Easter Island (Rapa Nui), integrating previous data of Vezzoli and Acocella (2009) and Gioncada et al. (2010), and showing sampling sites (IP) of this study. Notice that information regarding the three main polygenetic volcanoes (Poike, Rano Kau, and Terevaka) is separated from data related to small-volume monogenetic vents.

Poike Volcano (370 m asl) is located at the eastern end of the island (Fig. 2). Most of the edifice consists of a thick succession of lava flows exposed along the sea cliffs (Gioncada et al., 2010).

K/Ar geochronology dating of the volcano yielded ages ranging from 2.54 ± 0.28 Ma to 0.26±0.21 Ma (Baker et al., 1974; Clark, 1975; Kaneoka & Katsui, 1985). Rano Kau (300 m asl) is located at the southwestern end of the island and hosts a distinctive non-explosive central caldera currently filled with a lake (Fig. 2). K/Ar Ages from this volcano range from 0.94 ± 0.19 Ma to 0.34 ± 0.03 Ma (Clark, 1975; Miki et al., 1998) (Fig. 2), although field relationships suggested that volcanism here also started around 2.5 Ma (Gioncada et al., 2010). The Terevaka shield volcano (511 m asl) is located at the northern end of the island (Fig. 2). Most of the edifice consists of lava flows whereas the rifted summit is cross-cut by several NNE-SSW aligned craters (Rano a Roi the largest) on top of topographic ridges formed by coalescing and superposed scoria cones (Baker, 1967; Baker et al., 1974; Vezzoli & Acocella, 2009). (Gonzales-Ferran et al., 2004) considered Terevaka volcanism to span between ~1.9 and 0.3 Ma from field relationships, the latter relying on a K/Ar age of ~0.30 Ma reported by (Baker et al., 1974) without analytical data. Younger K/Ar ages of 0.14 ± 0.06 Ma and 0.12 ± 0.05 Ma were reported by (Clark, 1975) and belong to the late rifting stage of the central edifice (Vezzoli & Acocella, 2009).

The monogenetic vents (Fig. 2) formed during the rifting stage include (i) two NE-SW aligned phreatomagmatic basaltic tuff cones (P. E. Baker, 1967; Bonatti et al., 1977; Heyerdahl & Ferdon, 1961), (ii) seven evolved vents, comprising three trachyte-rhyolitic lava-domes, four obsidian lava-domes and an obsidian-breccia vent strongly aligned through NE-SW parallel structures and (iii) multiple NE-SW, NNE-SSW and NNW-SSE trending basaltic scoria cones cross-cutting the island (see electronic appendix in Gioncada et al., 2010 and in Vezzoli & Acocella, 2009).

The extrusion of evolved magmas is structurally controlled along the NE-SW faults crosscutting the southern polygenetic centers (Haase et al., 1997). The undated trachyte-rhyolite end-member cutting the northern slope of Poike include three lava domes (Maunga Vai a heva, Maunga Tea-tea, and Maunga Porehe; Baker, 1967; Baker et al., 1974; Bonatti et al., 1977). On the northeastern slopes of Rano Kau, there is an effusive and an explosive vent. The former is the well-known Maunga Orito lava-dome, which was K/Ar dated between 0.34 ± 0.06 Ma and 0.24 ± 0.03 Ma (Clark, 1975; Heyerdahl & Ferdon, 1961; Kaneoka & Katsui, 1985; Miki et al., 1998; Vezzoli & Acocella, 2009). The explosive vent corresponds to the Te Manavai crater, which is the source of a distinctive spherulitic, obsidian-rich tuff breccia (Baker, 1967). Vezzoli & Acocella (2009) reported K/Ar ages of 0.11 ± 0.04 Ma and 0.18 ± 0.003 Ma, which likely correspond to fragments derived from this explosive source. In addition, the NE-SW Motu-nui, Motu-iti, and Motu-kaokao islets, which emerged to the southwest of the island, also expose rhyolites and obsidian (Vezzoli & Acocella, 2009).

Dry basaltic, hawaiite, and mugearite scoria cones are the most common monogenetic vents across the island, following NNE-SSW, NNW-SSE, and NE-SW structural trends (Gioncada et al., 2010, in Gonzales-Ferran et al., 2004). The documented K/Ar ages for the monogenetic volcanism range from 0.24 ± 0.05 Ma to 0.09 ± 0.02 Ma (James Gregory Clark, 1975) without showing a specific trend in vent migration (see appendix in Vezzoli & Acocella, 2009).

3 Sampling, methods, and analytical procedures

During the reconnaissance field trip that lies at the basis of this paper, rock sampling was not allowed due to geoheritage restrictions. A total of twelve (12) detrital samples were collected, four from beach sands and eight from soil in the island's interior (Fig. 2). Of these, nine samples contain zircon grains (Table 1; Figs. 2 and 3). The sampling procedure included the selection of representative localities where sufficient soil and sand were available and that covered different potential source areas from the volcanic vents.

Tabelle 1 Sampling sites ‘with coordinates and general description.

Sample	Coordinates		Locality	Lithology	Comment
	Latitud	Longitud			
IP-1	S 27° 04' 23"	W 109° 19' 20"	Anakena beach	Beach sand	Distinct by its predominant bioclastic componentry compared to the rest of the studied localities
IP-2	S 27° 04' 26"	W 109° 18' 57"	Obahe beach	Beach sand	On the eastern flank of the scoria cones belonging to the polygon 19 in the Vezzoli and Acocella (2009) map.
IP-3	S 27° 08' 52"	W 109° 24' 59"	Vaihu beach	Beach sand	The samples are the product of erosion from regoliths on top of lava flows belonging to the NNW-SSE vents of the polygon 21 mapped by Vezzoli and Acocella (2009). Precense of pahoehoe lava-flows, locally showing pillow structures.
IP-4	S 27° 09' 56"	W 109° 21' 44"	Kona Ha'ari - Otongariki	Beach sand	Idem to IP-3
IP-5	S 27° 07' 12"	W 109° 14' 35"	Poike Volcanoe	Red soil	The red lateritic soil developed on top of the P1 aphyric to porphyritic lava flow succession forming the southeastern flanks of Poike shield volcano and exposed along the high sea cliffs
IP-7	S 27° 10' 45"	W 109° 24' 22"	Vinapu	Red soil	Red soil profile/regolith developed on top of a succession of bedded lava-flows exposed on the southeastern flanks of Rano Kau shield volcano. The sample overlays the unit mapped as R1 at Maunga Orito.
IP-8	S 27° 10' 12"	W 109° 24' 03"	On the road	Red soil	Red soil profile/regolith developed on top of a succession of bedded lava-flows exposed on the southeastern flanks of Rano Kau shield volcano. The sample overlays the unit mapped as R2, at Maunga Orito
IP-11	S 27° 05' 29"	W 109° 22' 52"	Terevaka Volcanoe	Red soil	Sample collected from the regolith developed on top of the youngest, NNE-SSW aligned scoria cones belonging to the unit mapped by Vezzoli and Acocella (2009) as T2a.
IP-12	S 27° 07' 24"	W 109°17' 29"	Ranu-Raraku	Soil	Sample collected from the regolith and locally washed epiclastic silts exposed on the western flank of the Rano Raraku tuff cone

All samples were panned with seawater directly on the island and only the heavy fraction was taken. The magnetic fraction of each sample was separated with a neodymium hand magnet and further panned with ethanol in the laboratory. Zircons for isotopic analysis were then handpicked during optical inspection under a binocular microscope and mounted in epoxy resin. The mount was ground down and polished to expose the interiors of the grains. Grains were photographed in reflected and transmitted light and under cathodoluminescence (CL; after carbon coating) to enable easy and best location for analytical spots during analysis. CL imaging was performed in the EMP (Electron Microprobe) facilities at Mainz University using a JEOL JXA-8200. Operating conditions were 20.0 kV and 30nA.

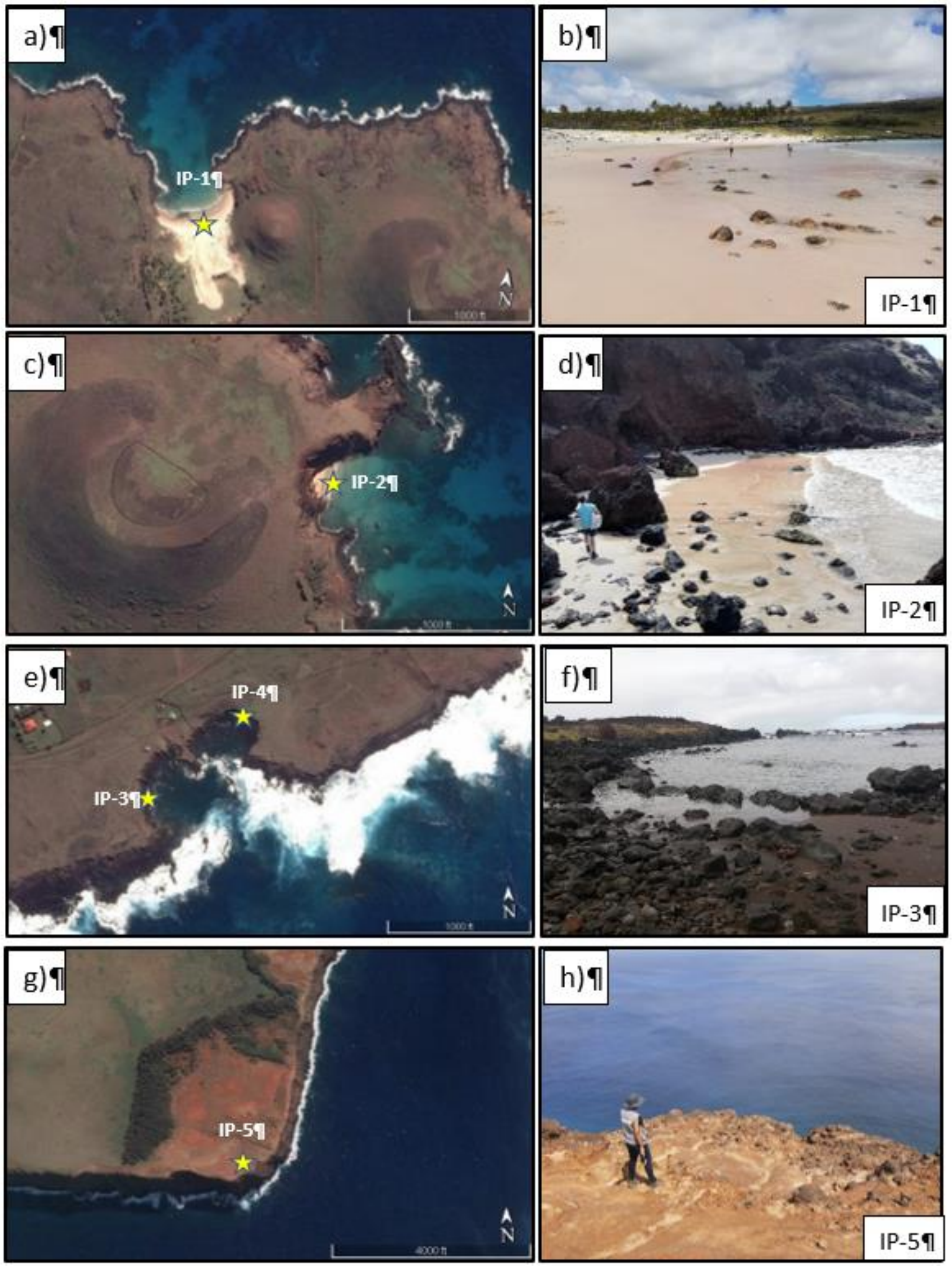

Figure 3 Google Earth images and photos of sample locations IP-1, IP-2, IP-3, and IP-5 (see the geological map on Fig. 2 for sample locations). a) Google Earth image of Anakena Beach, b) Photo of Anakena Beach, c) Google Earth image of Ovahe Beach, d) Photo of Ovahe Beach, e) Google Earth image of Vaihu (left) and Palmeras de Otongariki (right), f) Photo of Vaihu Beach, g) Google Earth image of clift southeast of Poike volcano, h) photo from red soil on the clift (150 m) southeast of Poike volcano

Zircon was analyzed in situ for U-Pb and Hafnium (Hf) at the laboratory facilities of the Frankfurt Isotope & Element Research Center (FIERCE, Germany), for Oxygen (O) at the SHRIMP II of the Beijing SHRIMP Centre, Chinese Academy of Geological Sciences and for trace elements at the laboratories of the State Key Laboratory of Lithospheric Evolution, Institute of Geology and Geophysics, Chinese Academy of Sciences. The results appear in Tables S2-S4. Analytical procedures are presented in detail in the -supporting Infirmation. A correction for initial ^{230}Th and U-series disequilibrium was applied to all zircon grains younger than 2 Ma (For more details see Rojas-Agramonte et al., 2017).

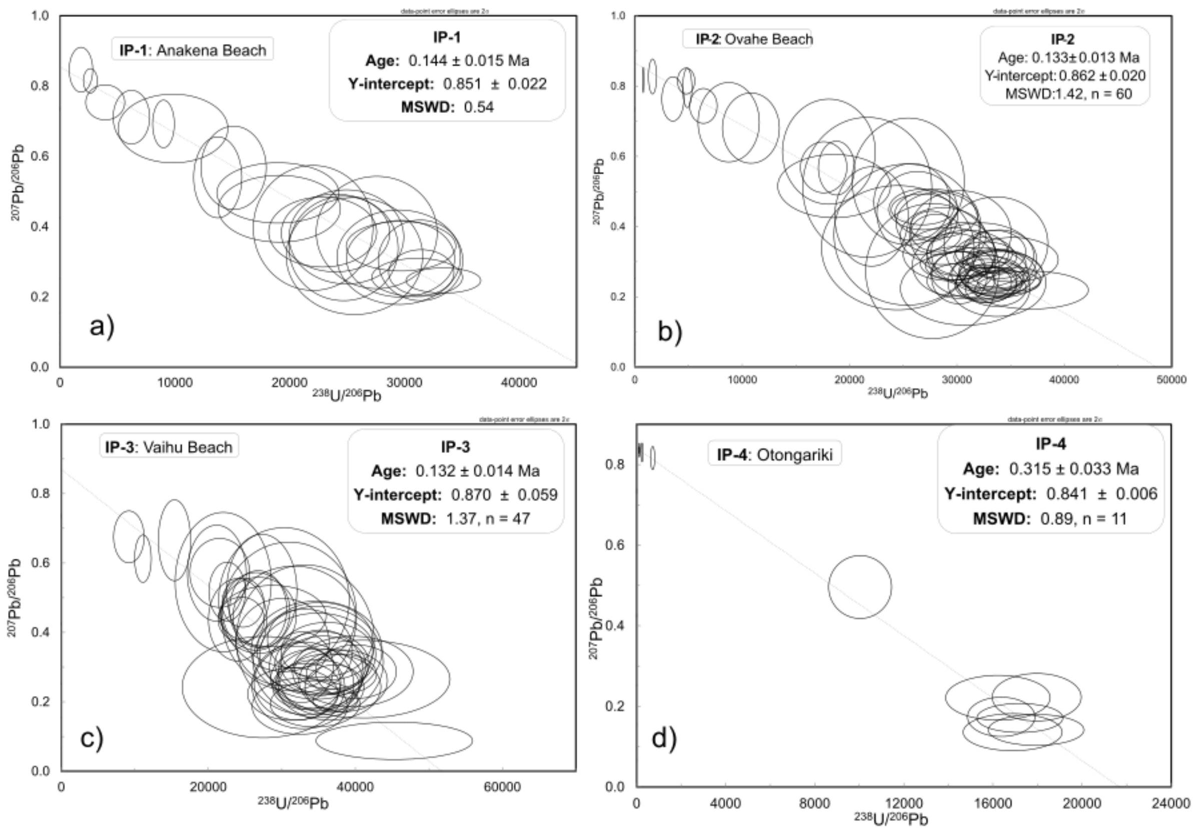

Figure 4 Concordia diagrams and U-Pb ages retrieved from zircons sampled in Rapa Nui beaches; a) IP-1 Anakena Beach, b) IP-2 Ovahe Beach, c) IP-3 Vaihu Beach, and d) IP-4 Otongariki site.

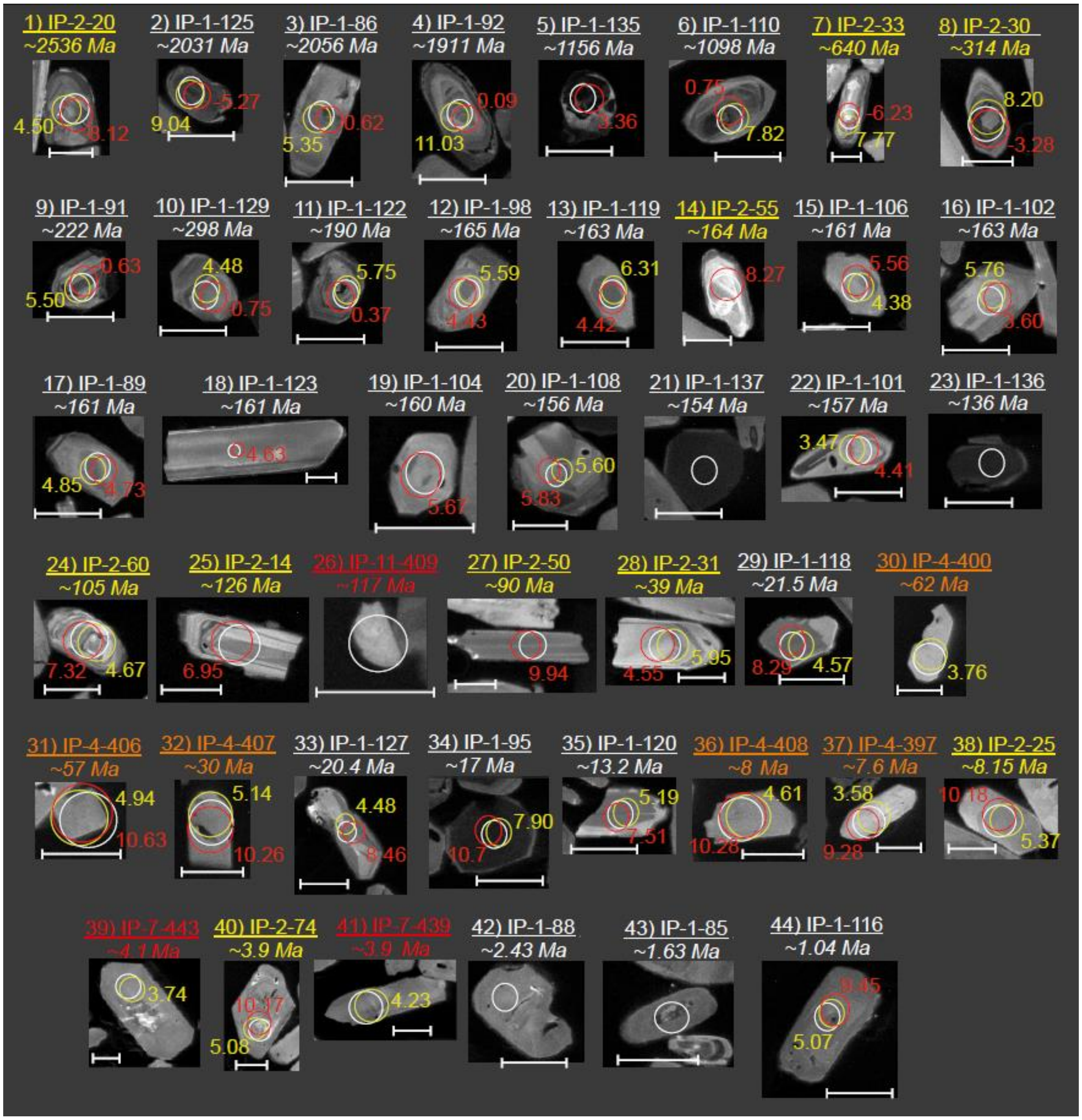

Figure 5 Cathodoluminescence images of zircons retrieved from each sample, marked in colors and organized from oldest (to) to youngest (bottom). Regions of interests for in situ analyses are marked as white circles for U-Pb, red circles for hafnium, and yellow circles for oxygen isotopic measurements.

4 Results

The sand on each beach in Easter Island is unique in composition, color, and grain size, as a result of biological activity, their source rocks, and coastal processes. The two main beaches on the island are located in the northern part (Ovahe and Anakena). White coral sands dominate the 210 m wide, sand-rich embayed beach in Anakena (Figs. 3a, b; sample IP-1). Dark/red volcanic-derived detritus dominates in the 70m wide Northern pocket beach Ovahe, forming soft sands in both (Figs. 3c, d; sample IP-2). The sediment-starved beaches of Vaihu in the south are dominated by dark volcanic-derived blocks and detritus (Figs. 3e, f; samples IP-3 and IP-4).

The soils of Easter are all of volcanic origin, derived either from pyroclasts or weathered volcanic rocks. The soils are red, yellow, or brown in color and in places appear slightly undulating with steep cliffs on some of the edges facing the sea, especially on the margins of the Rano Kao and Poike volcanoes (Figs. 3h, h, sample IP-5). Samples IP-7, IP-8, IP-11, and IP12 also come from red soils sampled across the island (Fig. 2). All samples contain a variable amount of zircon grains except for samples IP-11 and IP-12, where zircon is sparse (Figs. S9 and S10). Zircons older than the age of the volcanism of the island are concentrated in the north in samples IP-1 and IP-2 (Fig. 2). In sample IP-1 of 49 dated zircons 24 are old and in sample IP-2 of 76 dated zircons 9 are old (Table S2). In addition, sample IP-4 (contains 5 older zircons out of 16) and IP-5 with only one older zircon out of 75 dated. See detail description below.

4.1.1 In-situ U-Pb in zircon

Analyses were guided by cathodoluminescence (CL) images (Figs. S2 to S10 of the Supporting Information). The zircon crystals in the studied samples vary in size (from 100 up to 550 µm) and shape. Although most crystals are euhedral (equant to elongated), some are broken or rounded. In some cases, the zircons show oscillatory zoning. There is no clear correlation between zircon shape, size, and age group, although some of the oldest zircons appear with rounded terminations and clear core and rim features. The rims are too small to be dated by LA-ICP-MS (e.g. Fig. S2; spot number 92).

A total of forty-nine (49) grains were recovered from sample **IP-1** at the enclosed Anakena Beach (Figs. 3a, b; Table S2). These are mostly Pleistocene in age (n=24), between 2.43 ± 0.46 Ma and 0.19 ± 0.02 Ma, yielding a concordant age at 0.144 ± 0.015 Ma (Fig. 4a). One more grain yielded a Pliocene age (3.5 ±1.6 Ma) and the rest are significantly older. Four Miocene (21.5 ± 0.5 to 13.2 ± 0.3 Ma), one Lower Cretaceous (136 ± 7 Ma), eleven Jurassic (190 ± 5 to 154 ±10 Ma), one Upper Triassic (222 ± 5 Ma), one early Permian (298 ± 6 Ma), three Mesoproterozoic (1242 ± 20, 1156 ± 22, and 1098 ± 21 Ma), and three Paleoproterozoic (2059 ± 32, 2031 ± 38 and 1911 ± 38 Ma) grains were dated (Figs. 5 and S11).

A total of seventy-six (n = 76) grains were recovered from sample **IP-2**, at the enclosed Ovahe Beach (Figs. 3c, d). Most of them (n = 66) also provided Pleistocene ages between 1.82 ± 0.43 Ma and 0.17 ± 0.02 Ma, yielding a concordant age at 0.133 ± 0.013 Ma (Fig. 4b). One more grain is Pliocene (3.9 ± 0.7 Ma) in age, and the rest are significantly older. One Miocene (8.1 ± 0.4 Ma), one Eocene (39.1 ± 0.8 Ma), three Cretaceous (from 90.2 ± 2.0 to 126 ± 3 Ma), one Middle Jurassic (164 ± 3 Ma), one Middle Carboniferous (314 ± 6 Ma), one Neoproterozoic (640 ± 12 Ma), and one Early Paleoproterozoic (2536 ± 42 Ma) grains were dated (Figs. 5 and S11).

We recovered sixty-five (65) grains from sample **IP-3**, at Vaihu beach (Figs. 2 and 3e, f). All of them consistently provided Pleistocene ages between 0.38 ± 0.05 Ma and 0.11 ± 0.05 Ma, yielding a concordant age at 0.132 ± 0.014 Ma (Fig. 4c). The neighboring sample **IP-4** provided fourteen (14) grains. Ten (10) Pleistocene grains dated between 0.58 ± 0.12 Ma and 0.18 ± 0.01 Ma, yielding a concordant age of 0.315 ± 0.033 Ma (Fig. 4d). The other four grains yielded two

Miocene ages (8.4 ± 0.6 and 7.6 ± 0.4 Ma) and one Oligocene (29.6 ± 4.8 Ma) and one Paleocene (57.0 ± 9.1Ma) age (Fig. 5).

Sample **IP-5**, from a red soil from Poike volcano (Figs. 3g, h) contains a large amount of zircon grains (n =92). Most of the zircons provided Pleistocene ages between 1.70 ± 0.74 and 0.31 ± 0.04 Ma, yielding a concordant age of 0.310 ± 0.030 Ma (Fig. 6a) and one Eocene grain (49.4 ± 8.7 Ma; Fig. 5).

On Rano Kau flanks, most zircons recovered from lateritic soil in sample **IP-7** (n = 53), yielded a concordant Pleistocene age of 0.309 ± 0.030 Ma (ranging from 1.60 ± 0.34 to 0.418 ± 0.05) (Fig. 6b). Two other grains are Pliocene in age (4.10 ± 0.74 and 3.90 ± 1.05 Ma). In addition, a total of 27 grains were recovered from sample **IP-8**, yielding a concordant Pleistocene age of 0.309 ± 0.032 Ma (Fig. 6c), ranging between 1.184 ± 0.02 Ma and 1.184 ± 0.02 Ma.

Very few zircon grains were recovered from red soil at the summit of Terevaka (sample **IP-11)**. Only two grains were dated, one being Early Pleistocene (~2.27 ± 0.3 Ma) and the other one Cretaceous (117 ± 50 Ma; Fig. 5). Likewise, most of the heavy minerals recovered from black soil at Rano Raraku (sample **IP-12**) are apatite. The only zircon found was dated at 0.57 ± 0.19 Ma.

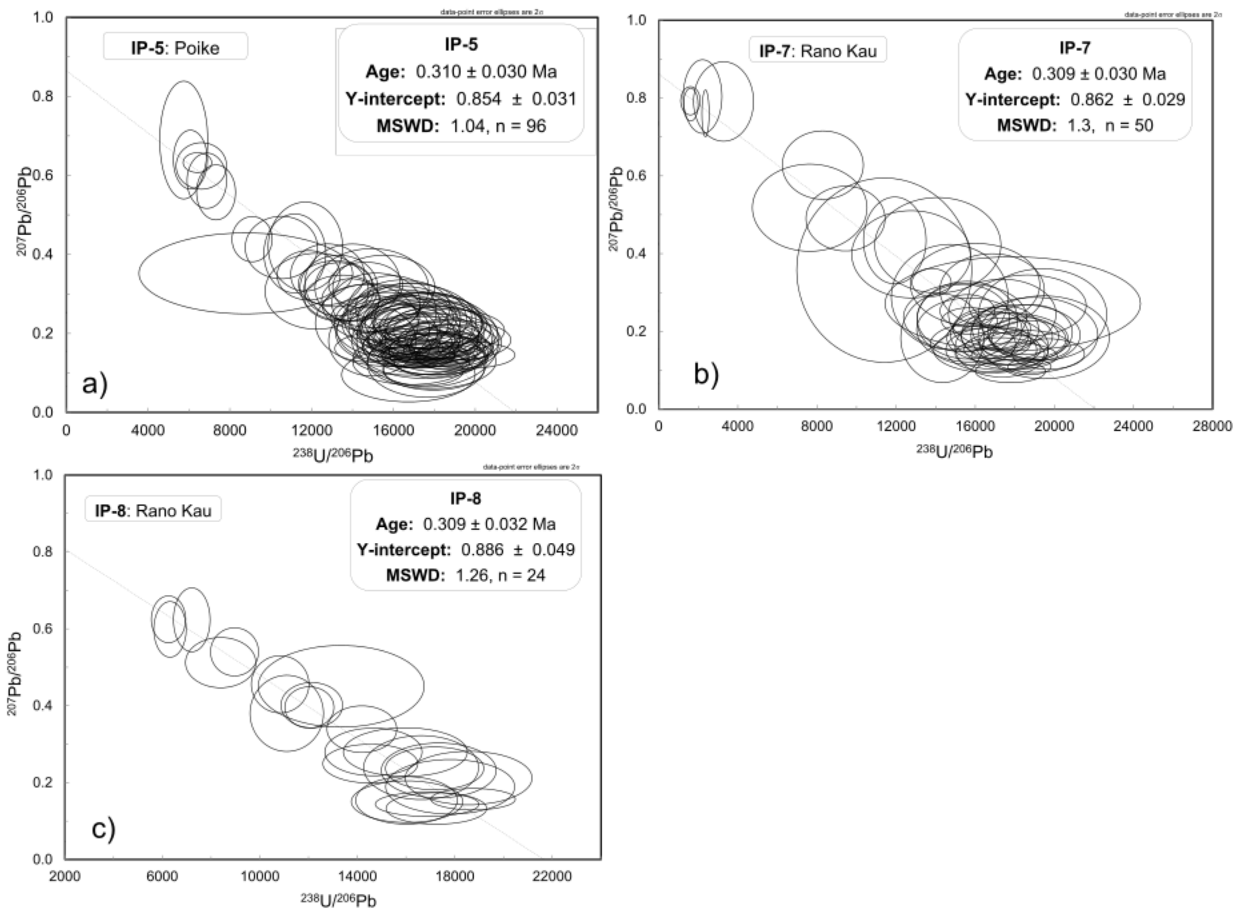

Figure 6 Concordia diagrams and U-Pb ages retrieved from zircons sampled on the flanks of the main shield polygenetic volcanoes; a) IP-5 at Poike, b) IP-7 at Rano Kau, and c) IP-8 at the limits between Ran Kau and Mt Orito.

4.1.2 Zircon Lu-Hf and Oxygen isotopes composition

The zircon $\varepsilon Hf_{(t)}$ and $\delta_{18}O_{(zircon)}$ values are plotted versus U-Pb age in Fig. 7A. All zircon grains with ages ~0 to 165 Ma exhibit a range of positive $\varepsilon Hf_{(t)}$ values (+3.5 to +12.5), however, most of the analysis have an average of $\varepsilon Hf_{(t)}$ = +8 to +10 (Figs. 7A and S12; Table S3). A small but distinct shift towards lower εHf compositions is observed as the grains become older compared to the younger zircon grains with lower values of +3.5 in the Jurassic grains (Fig. S12). Despite the spread in the εHf values these results reflect derivation from a predominantly juvenile depleted mantle source with the involvement of an isotopic heterogeneity in the source of the magmas. The oxygen isotope field for 'mantle' zircon (+5.3 ± 0.3‰; Valley, 2003) is shown for reference in Figs 7A and S12. Zircons younger than ~165 Ma show a modest range in $\delta_{18}O$ values between 3.8 and 5.9‰ except for one grain (~163 Ma) showing a more elevated value of 6.3‰. Approximately 25% of the zircons investigated plot within or straddle within error the mantle zircon field. An important feature revealed in these data is that the majority of the zircon oxygen isotope compositions plot below the mantle zircon reference field and indicate a more complex history of hydrothermal processes or interaction with high-T seawater in the upper part of the oceanic lithosphere (Valley, 2003). The isotopic composition of the zircon grains older than 164 Ma (Fig. 8) is characterized by more diverse and variable $\varepsilon Hf_{(t)}$ (-8.1 – +7.26) and $\delta^{18}O_{(zircon)}$ (4.4 – 11.3‰) values, consistent with both juvenile and continental crust signatures (Fig. 7A and S12; Table S4).

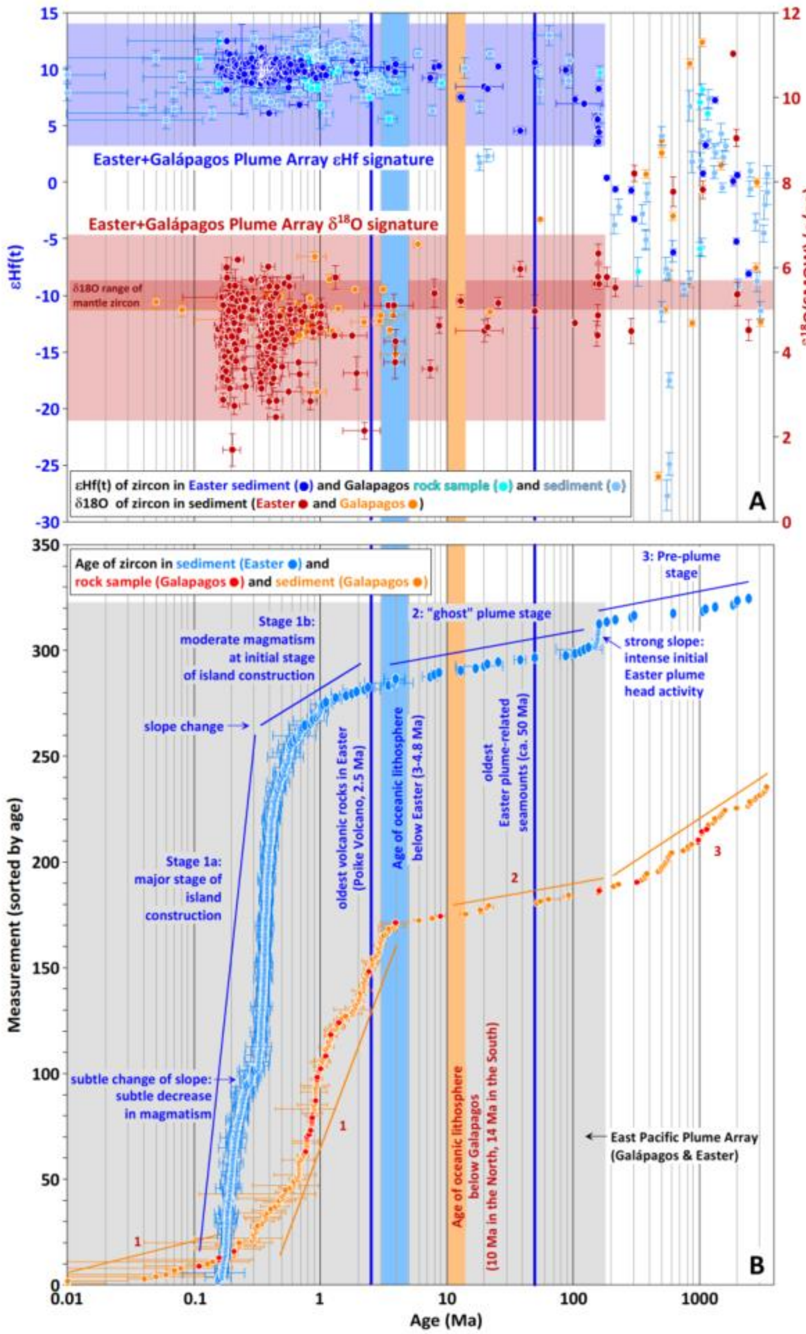

Figure 7 Isotopic composition (εHf(t) and δ18O(zircon)) and age of Easter zircons. The zircon data of Galápagos of Rojas-Agramonte et al. (2022) are also indicated for reference. (A) U-Pb age versus εHf(t) (bluish colors) and δ18O(zircon) (reddish colors) of analyzed zircons. The Easter+Galápagos Plume Array is defined by high εHf(t) and low δ18O(zircon), which extends from 0 Ma to 165 Ma (note significant scatter for Easter and Galápagos at >165 Ma). (B) Age of analyzed zircons sorted by age of spot. Note sectors with varied slopes denoting variable abundance of zircon ages for the corresponding time sectors.

4.1.3 Zircon trace element composition

Chondrite-normalized REE values are plotted by age range (~0–165 Ma and >165 Ma) in Fig. S13 and Table S5. Zircon younger than 165 Ma exhibits extreme enrichment in heavy rare earth elements (HREEs) relative to light rare earth elements (LREEs) and well-developed positive Ce anomalies and negative Eu anomalies (Fig. S13). These compositions are consistent with crystallization from very oxidized (~ 2 to 3 log10 orders *f*O2 > synthetic nickel-nickel oxygen buffer) magmas in which Eu^{2+} was extremely limited in abundance (Burnham and Berry, 2012; Trail et al., 2012). Uranium and Thorium abundances range from ~37 to ~1340 ppm and ~17 to ~1890 ppm, respectively (Table S5). Despite this wide range of concentrations, they form a well-defined array with a Th/U ratio that varies systematically from ~0.2 to ~2 with increasing U and Th. Hafnium concentrations are mainly between ~940 and ~15000 ppm. Zircons older than 165 Ma are less abundant and show REE patterns that display chondrite-normalized trends with enrichment in HREEs relative to LREEs and positive Ce and a less pronounced negative Eu anomalies compared to the younger grains (Fig. S13). Uranium and Thorium abundances display a narrower range compared to the younger zircon, ranging from ~134 to ~356 ppm and ~13 to ~122 ppm, respectively and a lower Th/U ratio ranging from 0.09 to 0.7 (Table S4; S5).

5 Discussion

5.1. Plio-Pleistocene ages

The Pliocene-Pleistocene ages constitute the vast majority (80%) obtained in this study (Figs. 8 and S14). They are within the range of K/Ar ages reported in the literature and show that zircon also crystallized from the magma that formed the volcano. Our results suggest that magmatism at Rapa Nui has been nearly continuous between 3.9 ± 0.74 and 0.11 ± 0.05 Ma. Pleistocene zircons retrieved from samples collected on the flanks of the main polygenetic volcanoes (IP-5, IP-7, and IP-8) consistently yielded concordant ages of ~0.3 Ma, whereas samples collected closer to the youngest monogenetic and fissure vents and products (IP-1, IP-2, and IP-3) yielded concordant ages at ~0.13–0.14 Ma.

After correlating our data with previous ages, the magmatism that yielded the construction of the main shields spanned from ~4.0 to ~0.6 Ma. Afterward, we identify a marked increase of ages between ~0.6 and ~0.3 Ma corresponding to the magmatism related to the caldera-stage volcanism identified by Vezzoli & Acocella (2009). Finally, magmatism driving the monogenetic and fissural volcanism cross-cutting the island likely started at ~0.51 Ma and is continuous down to 0.14 ± 0.03 Ma (Fig. S14). All data from monogenetic vents were treated separately because these sources are not necessarily related to the same reservoir-plumbing system as the three main edifices (Fig. 8). The oldest zircon age found at a monogenetic vent was retrieved at the Rano Raraku tuff cone (0.56 ± 0.19 Ma; IP-12), but we do not have an independent dating technique to constrain the onset of phreatomagmatism in the island. U/Pb ages between 0.51 ± 0.07 Ma (in IP-3) and 0.33 ± 0.08 Ma (in IP-1) show a good correlation with published K/Ar data for lavas of the early caldera stages at polygenetic volcanoes because our sampling sites correspond to the erosion products of the lavas and scoria cones mapped by Vezzoli & Acocella (2009). The concordia ages obtained at IP-7, IP-8, and IP4 suggest that dry mafic monogenetic volcanism was already occurring sometime around 0.309 ± 0.030 Ma and 0.315 ± 0.033 Ma. These results confirm the onset of the rifting stage of the island (Vezzoli & Acocella, 2009).

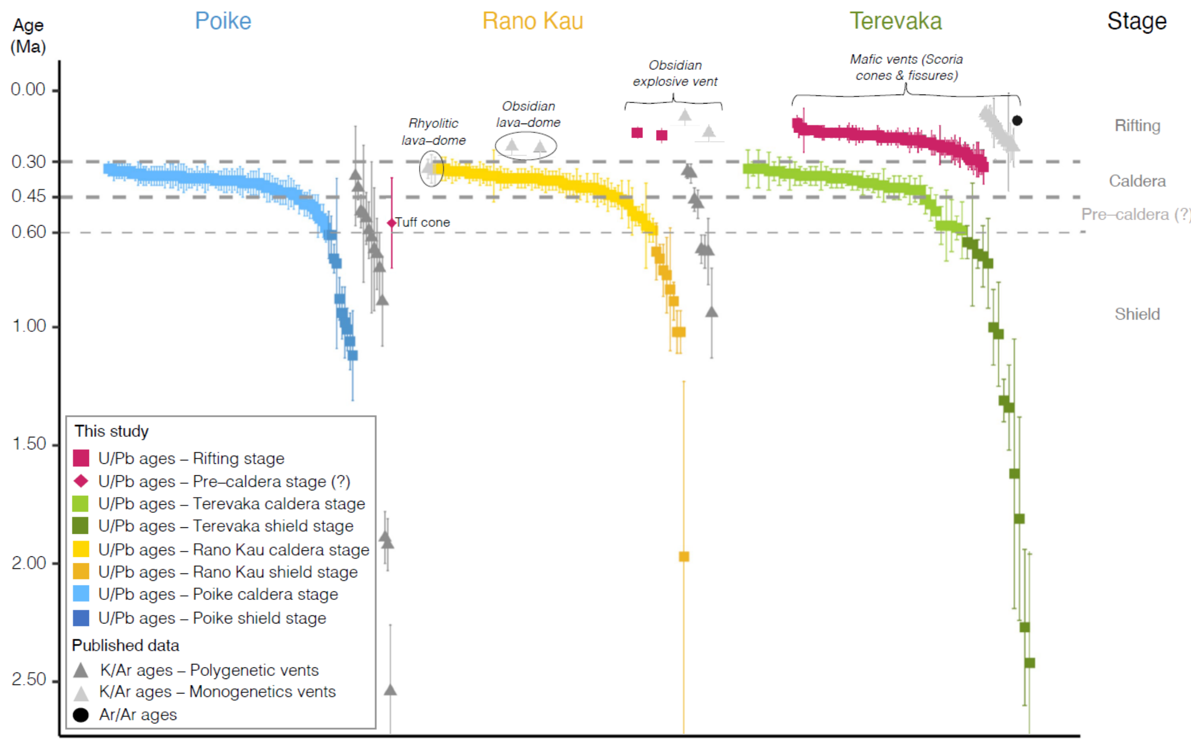

Figure 8 Geochronological database of Rapa Nui, summarizing previously published Ar^{40}/Ar^{39} and K^{40}/Ar^{40} ages, compare to our new U/Pb zircon ages (Table S6). Most of the data correspond to shield, pre-caldera, and caldera stages of each polygenetic central volcanoes. Younger ages corresponding to monogenetic vents formed during the rifting stage less represented and shown in detail Figure S14.

Consistently, evolved (rhyolitic) magmatism also started at ~0.3 Ma with the emission of rhyolitic lava-domes (dated by Gonzalez-Ferran and Baker, 1974; Miki et al., 1998) followed by ~0.2 Ma old obsidian lava domes dated by Kaneoka and Katsui (1985). The sampling locations and U/Pb ages of IP 7 (0.19 ± 0.03 Ma) and IP-8 (0.18 ± 0.02 Ma) clearly correlate with the 0.18 ± 0.03 Ma K/Ar age reported at the Te Manavai obsidian-rich explosive vent by Gonzalez-Ferran & Baker, 1974). All younger ages retrieved from locations close to scoria cones and the youngest mapped lava flows yielded ages between 0.30 ± 0.05 Ma (in IP-3) and 0.14 ± 0.03 Ma (in IP-3), with ~0.13–0.14 Ma concordant ages clearly correlating to the published data for the latest eruptions (Vezzoli & Acocella, 2009). Most zircons within this age group have positive εHf values between +6.1–12.5 (Table S3), indicating a predominantly juvenile-depleted mantle source.

The finding of zircons with crystallization ages older than the ~3.0–4.8 Ma age of the oceanic lithospheric basement cannot be explained by crystallization of the lavas on the island, or of the oceanic crust below the volcano. They occur mostly in the North (IP-1 and IP-2 with the highest age variability) and Southeast (IP-4). Zircon in the range ~4–165 Ma bear $\varepsilon Hf_{(t)}$ and $\delta^{18}O$ signatures typical of mantle zircon similar to the pre-4 Ma zircons (Figs. 7A and S12), showing that they come from the erosion of the mantle-derived volcanic products. The finding of zircon grains on hotspot-related islands that are much older than the age of volcanism in the island or the underlying oceanic crust (i.e., >4 Ma in the case of Easter Island) has far-reaching geodynamic implications if they were brought up from the underlying mantle as xenocrysts (Rojas-Agramonte et al., 2022). It is therefore important to consider whether the zircon cargo from the beaches and soils may have been transported from elsewhere. Possibilities are then aeolian, marine, or human transport. Aeolian transport should then transport zircons either blown by strong winds or volcanic eruptions.

Oceanic currents could transport zircons from the continent to Easter Island, which is located within the South Pacific Gyre, a large ocean current that is also responsible for the transport of plastics from the coast of Peru and Chile to the island (Gennip et al., 2019). Theoretically, old zircons could arrive on the island transported in or on plastic, or as part of large floating pumice rafts created by eruptions of submarine volcanoes (Jutzeler et al., 2020; Ohno et al., 2022). Finally, old zircons could have been transported to the island as ship ballast, or otherwise through human transport.

While contributions from these sources cannot be entirely excluded, it is hard to explain the zircon age distribution and chemistry with these alternative sources. The distance of Easter Island to the South American continent of ~3800 km makes airborne transport of zircon crystals with sizes of several hundred µm (Figs. S2 and S3) very unlikely. Even if the zircons would have been introduced through pumice rafts, the question remains how these old zircons ended up in the pumice. The coherent chemistry of the zircons of the last 165 Ma does not have an obvious source in South America, where they would have much more diverse isotopic signatures (signaling Andean volcanism, e.g., Balgord, 2017; Pankhurst et al., 2016) than those found in the present study. A key test to demonstrate that the zircons are derived from the volcano is the finding of a zircon cargo within the lavas that are comparable to those of the soils and beach sands. Such confirmation that sands and lavas from hotspot islands carry similar zircon cargo was shown elsewhere, on Galápagos (Rojas-Agramonte et al., 2022), and Mauritius (Ashwal et al., 2017; Torsvik et al., 2013). Nonetheless, natural processes such as erosion and detrital sediment accumulation, sorting, and temporary and past deposition are efficient ways to concentrate zircons in oceanic island environments (Rojas-Agramonte et al., 2022; Rojas-Agramonte et al., 2017; Seelos et al., 2021; Sevastjanova et al., 2011). Bearing in mind that we have not been able yet to demonstrate the *in-situ* presence of zircons xenocrysts in the Easter Island lavas, we will in the remainder of this discussion explore the implications of our findings assuming that they represent xenocrysts from the sublithospheric mantle below the volcano. Besides the hot-spot effusive eruptions typical of polygenetic shield volcanoes, monogenetic volcanism is known to be an excellent feeder mechanism able to drag deep accessory and accidental grains from their asthenospheric source to the surface (Brenna et al., 2011; R. Gao et al., 2017; Simon et al., 2008).

Early Jurassic (~190 Ma), Triassic (~222 Ma), Carboniferous (~314 Ma), and Precambrian (~640 to 2500 Ma) zircon ages retrieved at Rapa Nui are not expected in the oceanic crust. Most of the zircon grains older than 165 Ma have values ranging from 0 to negative εHf isotopic signatures typical of continental magma sources or of contamination with continental crustal material. Only two grains point toward a juvenile source (Fig. 7A). Such ancient zircons with diverse compositions were also reported from Galápagos (Rojas-Agramonte et al., 2022) and Hawai'i (Greenough et al., 2021) and are best explained as detrital zircons that were brought into the mantle by subduction. Whereas Galápagos is located in the vicinity of a subducted slab in the underlying lower mantle that subducted in the Mesozoic (the Malpelo slab, Van der Meer et al., 2018) no slabs are known below Hawaii and Easter Island. If these zircons resulted from subduction, they were either transported over large distances by mantle flow (Greenough et al., 2021), or they were introduced into the mantle when continents were still nearby. The geochemistry of central Pacific hotspots reveals geochemical traces of subducted continental crust that is widely thought to be present in the plume source at the core-mantle boundary and that subducted in the late Precambrian to early Paleozoic (e.g., Jackson & Macdonald, 2022) This would suggest that these xenocrysts may have been trapped in the upper mantle for hundreds of millions of years (Greenough et al., 2021; van Hinsbergen et al., 2020; Rojas-Agramonte et al., 2022), likely enclosed within mineral grains that provides a way to remain stable under asthenospheric conditions (Bea et al., 2020; Cambeses et al., 2023).

The ~165–0 Ma zircon, with clear Hf and O isotopic mantle signatures and well-covered age range from ~0–165 Ma appears to date the production of magmas for an extended period of time in the location of the current hotspot. The most straightforward explanation is that the current volcano is located at the site of a long-lived hotspot that dates back to the Middle Jurassic (~165 Ma). The pre-Pliocene zircons then likely represent minerals that formed and were stored in the asthenosphere, and that were picked up at sublithospheric depths by rising hot-spot magmas. Interestingly, this age range of hotspot-related zircons is similar to the one reported from Galápagos (Rojas-Agramonte et al., 2022), suggesting that both hotspots may date back to the middle Jurassic.

Figure 7B clearly shows different stages that we interpret as plume development and oceanic island formation of Easter Island compared to the recent findings in the Galapagos Archipelago. The younger stages are the island-formation events, with stage 2 which is the most recent and vigorous, denoted by the steep slope. This stage is characterized by the abundance of young zircons (<1 Ma), related to the majority of exposed rocks that are subject to erosion. Stage 2a is older and less vigorous (<3 Ma; not so many zircons for a larger time interval), as denoted by the less steep slope of the curve. Stage 1, which we dub the "ghost" plume stage, contains the xenocrysts and ends with the formation of oceanic lithospheres on which the modern islands are built. It is characterized by a fewer occurrence of zircons during the long period of time of plume activity (Fig. 7B: gentle slope). The gentle-slope curve extends to ages younger than the corresponding lithosphere, but these zircons do not correspond to stage 2 island-forming lavas zircons, but to older asthenospheric or lithospheric zircons recovered from lavas erupted later during stage 2. This “ghost” stage appeared to have abruptly started in the Jurassic with a strong slope. corresponding to a relative abundance of zircons (n = 8) for a relatively short time interval (156–165 Ma) at the beginning of the EPPA. We postulate that this was related to the first arrival of the plume head below the lithosphere, which could then have generated a Large Igneous Province (LIP).

The lithosphere that was present above the present-day locations of the Easter and Galápagos hotspots has long been lost to subduction, but we perform an experiment to evaluate where the hypothetical, ~165 would have subducted. We will use this to test whether a geological record of this LIP, or of the effects of its subduction, may still be present in circum-Pacific orogens.

The arrival of LIPs in trenches is known to have major tectonic effects. The arrival of the Ontong-Java plateau at the Melanesian trench caused strong upper plate deformation that even led to subduction polarity reversals (e.g. Knesel et al., 2008). However, accretion of crustal units from LIPs is rare, probably because there are few horizontal decollement horizons in the dyke-pierced LIPs, and they eventually tend to entirely subduct (Van Hinsbergen & Schouten, 2021) or only leave minor accreted ocean plate stratigraphy thrust slices (van de Lagemaat et al., 2023). Hence, we may evaluate whether, around the time interval in the location of predicted subduction, there is a record of upper plate shortening.

For our reconstruction (Fig. 9), we use a recently updated plate model of the southern Pacific region back to the early Cretaceous (van de Lagemaat et al., 2023), and a simple plate model based on mirroring the Early Cretaceous and Late Jurassic magnetic anomalies preserved in the Pacific plate prior to that (Boschman et al., 2021). The relative motions between the Pacific plate and its oceanic neighbors and the Pangea-derived continents of the Indo-Atlantic plate system is directly constrained through a connection to Antarctica for the last 83 Ma (e.g. Torsvik & Cocks, 2019). However, prior to this connection, the Pacific Ocean plates and the surrounding continents were everywhere separated by trenches or transforms, and relative motions between these plate systems relies on independent mantle reference frames. For the Pacific plate, we use the latest fixed hotspot frame of Torsvik et al. (2019), which extends back in time to 150 Ma, and for the Indo-Atlantic plate system we use the slab-fitted reference frame of that is the only one that goes back to the Jurassic. (Boschman et al., 2019) showed that these two reference frames perform well in predicting paleomagnetic and age grid constraints for the transition of the Caribbean plate from the Pacific to the Indo-Atlantic plate systems around 100 Ma. Before 150 Ma, we use the approximate position of the Pacific and neighboring oceanic plates relative to the Indo-Atlantic plates that was estimated by Boschman et al., 2021) that was chosen such that subduction is maintained at all trenches surrounding the Panthalassa ocean. The uncertainty in the position of the Pacific relative to the Indo-Atlantic plates is difficult to quantify, but is likely on the order of 500–1000 km. Hence, the absolute ages that we estimate below should not be taken too literally, but the uncertainty has little effect on the region and the general timing of subduction of the LIPs.

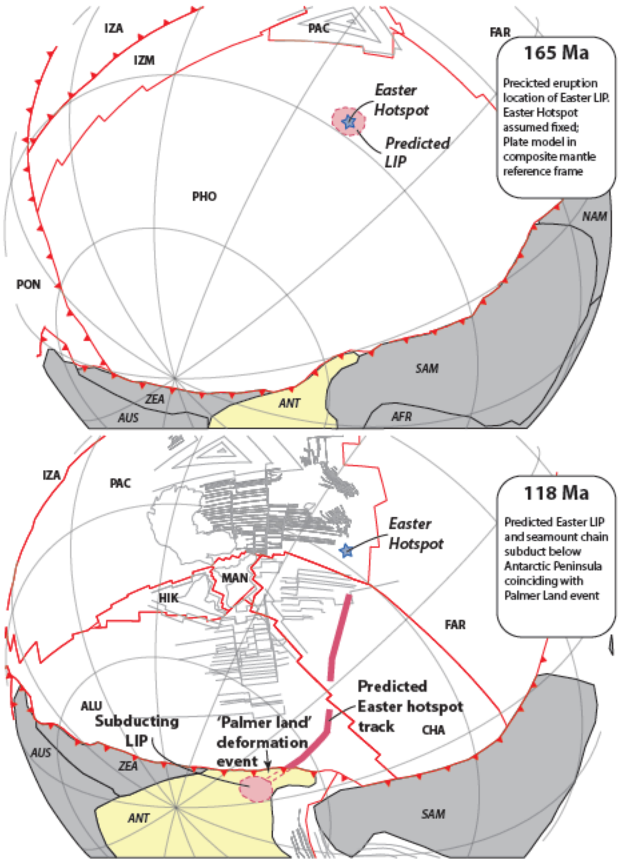

Figure 9 A) Paleogeographic reconstructions of the southern Pacific realm in a composite mantle reference frame (see text), indicating the predicted location of the Easter LIP at 165 Ma, assuming that the Easter hotspot has remained mantle-stationary. B) The plate model predicts that the 165 Ma-old Easter LIP would have subducted around 118 Ma below the Antarctic Peninsula, followed by the subduction of an associated seamount chain until ~108 Ma. This coincides with the enigmatic Palmer Land deformation event on the Antarctic Peninsula.

For our reconstruction, we assume that the Galápagos and Easter hotspots have remained stationary in the mantle since 165 Ma. We then draw a circular LIP around the location of the hotspot at 165 and attach it to the plate that was at that time located above the hotspot. For the Galápagos hotspot, this was the Farallon plate, likely just north of the Farallon-Phoenix ridge, and for the Easter hotspot, this was the Phoenix Plate. The Galapagos LIP would likely have been located in the lithosphere that was consumed by Early Cretaceous subduction below the intra-oceanic subduction zone whose remains are found in the northern Caribbean region, from Guatemala over Cuba to Hispaniola. The Cuban ophiolites have been intensely deformed after the Early Cretaceous (e.g. Iturralde-Vinent et al., 2016), and while Early Cretaceous upper plate deformation may well have occurred, there is no possibility to confirm or exclude this scenario.

Our reconstruction shows that the hypothetical Easter LIP would have subducted below the Antarctic Peninsula, starting around 120 Ma, and a hypothetical seamount chain would have subducted below the Peninsula until ~110–105 Ma (Fig. 9). After that, the seamount chain would have subducted below South America. Interestingly, this coincides with the enigmatic 'Palmer Land' deformation event (Vaughan et al., 2002). This deformation comprises NW-SE shortening that started at or before 116 Ma, and that ended around 106 Ma, by which time the deformed rocks were unconformably covered by undeformed arc sequences (Vaughan et al., 2002, 2012). Vaughan et al. (2002, 2012) inferred that this deformation was likely the result of the arrival of a buoyant indenter at the trench, but no accretionary geological record has so far been recognized. The subduction of a 165 Ma Easter LIP and following would provide a straightforward explanation for this poorly understood shortening event.

It is early days to use zircon xenocrystic cargo as basis for geodynamics, and there are many sampling targets in the oceans that may provide a wealth of new information. Nonetheless, we consider our test of whether zircon cargo from remote oceanic islands can offer a new geodynamic perspective to be positive. Our findings provide a second example of what we hypothesize is the ghost of a prolonged plume history, and the coincidence of the predicted LIP subduction and the Palmer Land deformation event is striking. If our hypothesis is valid, the geodynamic implications are far reaching. It would suggest that not only the Galápagos and Easter hotspots are nearly mantle-stationary, but also that the asthenosphere in which the underlying plume is contained did not appreciably move for the last 165 Ma. Because if the mantle would convected and moved laterally with a plume fed from below continuously piercing 'fresh' asthenosphere, the older melt relics and zircon cargo would have convected away. Previously, geochemical traces of subduction found in young volcanic rocks that were unrelated to subduction were linked to detached slabs in the underlying mantle, suggesting that former 'ghost' mantle wedges are still located above the slabs that made them, 10's to 100's of Ma after slab breakoff (Gianni et al., 2023; van Hinsbergen et al., 2020; Richter et al., 2020). The finding of two 165 Ma long plume records below Galápagos (Rojas-Agramonte et al., 2022) and Easter Island (this paper) provides further arguments towards this surprising finding. Whereas we consider our findings preliminary, and more data and experiments will likely be needed to unlock the full potential of mantle-derived zircon xenocrysts, we conclude that our study provides ample reason to build a much larger database of intra-oceanic volcanic island zircon cargo.

6 Conclusions

Recent serendipitous findings of zircon xenocrysts in intraplate volcanic islands such as Hawai'i and Galápagos led us to test whether such a cargo is common and may be used as a novel source of information for geodynamics. Here we report zircons that we collected from beach sands and soils of Easter Island (Rapa Nui), a remote hotspot island 3800 km west of the South American mainland. Approximately 80% of these zircons returned U/Pb ages that coincide with the previously constrained ages of volcanism and the age of the underlying oceanic crust. However, 20% is considerably older and falls in two populations. One population of zircons with a spike of 165 Ma and covering the 165–4 Ma interval has coherent oxygen ($\delta_{18}O_{(zircon)}$) and hafnium mantle isotopic signatures ($\varepsilon Hf_{(t)}$), consistent with crystallization of zircon from plume-related melts. An older population dates back to the Archean and has diverse chemistries that point to a continental source. We postulate that the older zircons may relate to phases of subduction that occurred when continents still occupied this region in Paleozoic and older times, and suggests that zircon xenocrysts may survive in the asthenosphere for 100s of Ma, echoing previous conclusions. The ~165–4 Ma population would be straightforwardly explained by crystallization from melts generated by the Easter Hotspot, which would then have initiated ~165 Ma ago, long before the oldest, ~48 Ma relics identified in the geological record. We postulate that the population of ~165 Ma zircons could signal an intense initial massive melting phase associated with the impingement of the plume at the base of the lithosphere forming a Large Igneous Province (LIP). Using plate reconstructions, we show that this hypothetical LIP would have formed on the Phoenix Plate and subducted beneath the Antarctic Peninsula between ~120 and 105 Ma. This coincides with the enigmatic Palmer Land deformation event that started before 116 Ma, and ended around 106 Ma, previously proposed to result from the collision of an unknown indenter. Our findings show that asthenospheric mantle-derived xenocryst zircon cargo, such as that recently reported from Galapagos and Hawai'i, may not be an exception. The "ghost" of prolonged hotspot activity described here suggests that the Easter hotspot as well as the sublithospheric mantle in which it is located remained stationary for some 165 Ma, which, if true, has major implication for our understanding of mantle convection Even though we consider our results preliminary, we conclude that zircon geochronology combine with elemental (REE) and isotopic studies of young oceanic islands may offer a novel source of information that could upset our thinking of global-scale geodynamics.

Acknowledgments

We thank the whole Mauna Henua community for their hospitality, Rafael (Hamoa) Rapu, Reina Rapu, and Manu Iri for his field assistance. YRA and NP acknowledge funding from the Fondo de Profesores Asociados (FAPA) de la Universidad de los Andes (Colombia). YR-A acknowledges funding from Deutsche Forschungsgemeinschaft (DFG) grant RO4174/3-1 and RO4174/3-3 and SYNTHESYS and AG-C to the MICINN PID2019-105625RB-C21 and Junta de Andalucía PY20_00550. DJJvH acknowledges NWO Vici grant 865.17.001, and thanks Alex Burton-Johnson for discussions about Antarctic Peninsula geology. This is FIERCE contribution No. XX. It is also the appropriate place to thank colleagues and other contributors. AGU does not normally allow dedications.

Open Research

All the underlying data needed to understand, evaluate, and build upon the reported research are supply in the supporting information.

References

Aitchison, J. C., Cluzel, D., Ireland, T. R., Zhou, R., Lian, D., Patias, D., et al. (2022). Solid-phase transfer into the forearc mantle wedge: Rutile and zircon xenocrysts fingerprint subducting sources. *Earth and Planetary Science Letters*, *577*, 117251. https://doi.org/10.1016/j.epsl.2021.117251

Ashwal, L. D., Wiedenbeck, M., & Torsvik, T. H. (2017). Archaean zircons in Miocene oceanic hotspot rocks establish ancient continental crust beneath Mauritius. *Nature Communications*, *8*, 1–9. https://doi.org/10.1038/ncomms14086

Baker, P. E. (1967). Preliminary Account of Recent Geological Investigations on Easter Island. *Geological Magazine*, *104*(2), 116–122. https://doi.org/10.1017/S0016756800040577

Baker, Peter E, Buckley, F., & Holland, J. (1974). Petrology and geochemistry of Easter Island. *Contributions to Mineralogy and Petrology*, *44*(2), 85–100.

Bandy, M. C. (1937). Geology and petrology of Easter Island. *Bulletin of the Geological Society of America*, *48*(11), 1589–1610.

Bea, F., Montero, P., & Palma, J. F. M. (2018). Experimental evidence for the preservation of U-Pb isotope ratios in mantle-recycled crustal zircon grains. *Scientific Reports*, *8*(1), 1–10. https://doi.org/10.1038/s41598-018-30934-4

Bea, F., Bortnikov, N., Montero, P., Zinger, T., Sharkov, E., Silantyev, S., et al. (2020). Zircon xenocryst evidence for crustal recycling at the Mid-Atlantic Ridge. *Lithos*, *354–355*, 105361. https://doi.org/10.1016/j.lithos.2019.105361

Bello-González, J. P., Contreras-Reyes, E., & Arriagada, C. (2018). Predicted path for hotspot tracks off South America since Paleocene times: Tectonic implications of ridge-trench collision along the Andean margin. *Gondwana Research*, *64*, 216–234. https://doi.org/10.1016/j.gr.2018.07.008

Bjerga, A., & Pedersen, L. R. (2021). Inherited Continental Zircons in Oceanic Rocks – True or False, (August).

Bjerga, A., Stubseid, H. H., Pedersen, L.-E. R., Beinlich, A., & Pedersen, R. B. (2022). A highly depleted and subduction-modified mantle beneath the slow-spreading Mohns Ridge. *Geochemistry, Geophysics, Geosystems*, *23*(11), e2022GC010585.

Bonatti, E., Harrison, C. G. A., Fisher, D. E., Honnorez, J., Schilling, J.-G., Stipp, J. J., & Zentilli, M. (1977). Easter Volcanic Chain (southeast Pacific): A mantle hot line. *Journal of Geophysical Research (1896-1977)*, *82*(17), 2457–2478. https://doi.org/10.1029/JB082i017p02457

Bortnikov, N. S., Sharkov, E. V., Bogatikov, O. A., Zinger, T. F., Lepekhina, E. N., Antonov, A. V., & Sergeev, S. A. (2008). Finds of young and ancient zircons in gabbroids of the Markov Deep, Mid-Atlantic Ridge, 5°54′–5°02.2′ N (Results of SHRIMP-II U-Pb Dating): Implication for deep geodynamics of modern oceans. *Doklady Earth Sciences*, *421*(1), 859–866. https://doi.org/10.1134/S1028334X08050334

Boschman, L., Van der Wiel, E., Flores, K. E., Langereis, C., & van Hinsbergen, D. J. (2019). The Caribbean and Farallon plates connected: Constraints from stratigraphy and paleomagnetism of the Nicoya Peninsula, Costa Rica. *Journal of Geophysical Research: Solid Earth*, *124*(7), 6243–6266.

Boschman, L. M., Van Hinsbergen, D. J., Langereis, C. G., Flores, K. E., Kamp, P. J., Kimbrough, D. L., et al. (2021). Reconstructing lost plates of the Panthalassa Ocean through paleomagnetic data from circum-Pacific accretionary orogens. *American Journal of Science*, *321*(6), 907–954.

Boven, A., DeDapper, M., DePaepe, P., Langohr, R., & Pasteels, P. (1997). Evolution of the southwestern edge of the Poike volcano, Easter Island.

Brenna, M., Cronin, S. J., Németh, K., Smith, I. E. M., & Sohn, Y. K. (2011). The influence of magma plumbing complexity on monogenetic eruptions, Jeju Island, Korea. *Terra Nova*, *23*(2), 70–75. https://doi.org/10.1111/j.1365-3121.2010.00985.x

Burke, K., Steinberger, B., Torsvik, T. H., & Smethurst, M. A. (2008). Plume Generation Zones at the margins of Large Low Shear Velocity Provinces on the core–mantle boundary. *Earth and Planetary Science Letters*, *265*(1), 49–60. https://doi.org/10.1016/j.epsl.2007.09.042

Cambeses, A., Chakraborty, S., Jöns, N., Montero, P., & Bea, F. (2023). How does inherited zircon survive in partially molten mantle: Insights on modes of magma transport in the mantle from nanoscale melt-crystal interaction experiments. *Earth and Planetary Science Letters*, *601*, 117911. https://doi.org/10.1016/j.epsl.2022.117911

Chubb, L. J. (1933). Geology of Galápagos, Cocos, and Easter islands. Geología de las Islas Galápagos, del Coco e islas orientales. *Bernice P. Bishop Museum Bulletin.*, (110), 1–67.

Clark, James G., & Dymond, J. (1977). Geochronology and petrochemistry of Easter and Sala y Gomez Islands: implications for the origin of the Sala y Gomez Ridge. *Journal of Volcanology and Geothermal Research*, *2*(1), 29–48. https://doi.org/10.1016/0377-0273(77)90014-2

Clark, James Gregory. (1975). Age, chemistry, and tectonic significance of Easter and Sala y Gomez Islands.

Condie, K. C., Belousova, E., Griffin, W., & Sircombe, K. N. (2009). Granitoid events in space and time: constraints from igneous and detrital zircon age spectra. *Gondwana Research*, *15*(3–4), 228–242.

Courtillot, V., Davaille, A., Besse, J., & Stock, J. (2003). Three distinct types of hotspots in the Earth's mantle. *Earth and Planetary Science Letters*, *205*(3–4), 295–308. https://doi.org/10.1016/S0012-821X(02)01048-8

DePaepe, P., & Vergauwen, I. (1997). New petrological and geochemical data on Easter Island.

Domeier, M., Magni, V., Hounslow, M. W., & Torsvik, T. H. (2018). Episodic zircon age spectra mimic fluctuations in subduction. *Scientific Reports*, *8*(1), 17471.

Espurt, N., Baby, P., Brusset, S., Roddaz, M., Hermoza, W., Regard, V., et al. (2007). How does the Nazca Ridge subduction influence the modern Amazonian foreland basin? *Geology*, *35*(6), 515–518. https://doi.org/10.1130/G23237A.1

Gao, M.-H., Liu, P.-P., Chung, S.-L., Li, Q.-L., Wang, B., Tian, W., et al. (2022). Himalayan zircons resurface in Sumatran arc volcanoes through sediment recycling. *Communications Earth & Environment*, *3*(1), 283. https://doi.org/10.1038/s43247-022-00611-6

Gao, R., Lassiter, J. C., & Ramirez, G. (2017). Origin of temporal compositional trends in monogenetic vent eruptions: Insights from the crystal cargo in the Papoose Canyon sequence, Big Pine Volcanic Field, CA. *Earth and Planetary Science Letters*, *457*, 227–237. https://doi.org/10.1016/j.epsl.2016.10.013

Gennip, S. J. V., Dewitte, B., Garçon, V., Thiel, M., Popova, E., Drillet, Y., et al. (2019). In search for the sources of plastic marine litter that contaminates the Easter Island Ecoregion. *Scientific Reports*, *9*(1), 1–13.

Gianni, G. M., Likerman, J., Navarrete, C. R., Gianni, C. R., & Zlotnik, S. (2023). Ghost-arc geochemical anomaly at a spreading ridge caused by supersized flat subduction. *Nature Communications*, *14*(1), 2083.

Gioncada, A., Gonzalez-Ferran, O., Lezzerini, M., Mazzuoli, R., Bisson, M., & Rapu, S. A. (2010). The volcanic rocks of Easter Island (Chile) and their use for the Moai sculptures. *European Journal of Mineralogy*, *22*(6), 855–867.

Gonzales-Ferran, O., Mazzuoli, R., & Lahsen, A. (2004). Geología del complejo volcánico Isla de Pascua, Rapa Nui, Chile, V Región Valparaiso. Carta Geológica-Volcánica Isla de Pascua.

Gonzalez-Ferran, O., & Baker, P. E. (1974). Isla de Pascua. Field guide book, including the first easter island geological map 1: 50.000. In *IAVCEI International Symposium, Santiago, Chile* (Vol. 32).

González-Jiménez, J. M., Camprubí, A., Colás, V., Griffin, W. L., Proenza, J. A., O'Reilly, S. Y., et al. (2017). The recycling of chromitites in ophiolites from southwestern North America. *Lithos*, *294–295*, 53–72. https://doi.org/10.1016/j.lithos.2017.09.020

Greenough, J. D., Kamo, S. L., Davis, D. W., Larson, K., Zhang, Z., Layton-Matthews, D., et al. (2021). Old subcontinental mantle zircon below Oahu. *Communications Earth & Environment*, *2*(1), 1–9. https://doi.org/10.1038/s43247-021-00261-0

Haase, K. M., Stoffers, P., & Garbe-Schönberg, C. D. (1997). The petrogenetic evolution of lavas from Easter Island and neighbouring seamounts, near-ridge hotspot volcanoes in the SE Pacific. *Journal of Petrology*, *38*(6), 785–813.

Hagen, R. A., Baker, N. A., Naar, D. F., & Hey, R. N. (1990). A SeaMARC II survey of recent submarine volcanism near Easter Island. *Marine Geophysical Researches*, *12*(4), 297–315.

Hampel, A. (2002). The migration history of the Nazca Ridge along the Peruvian active margin: a re-evaluation. *Earth and Planetary Science Letters*, *203*(2), 665–679.

Harpp, K. S., Hall, P. S., & Jackson, M. G. (2014). Galápagos and Easter. In *The Galápagos* (pp. 27–40). American Geophysical Union (AGU). https://doi.org/10.1002/9781118852538.ch3

Heyerdahl, T., & Ferdon, E. N. (1961). Reports of the Norwegian Archaeological Expedition to Easter Island and the East Pacific. Volume 1. Archaeology of Easter Island. *Santa Fe: The School of American Research and the Museum of New Mexico.*, (24), 1–559.

Iturralde-Vinent, M. A., García-Casco, A., Rojas-Agramonte, Y., Proenza, J. A., Murphy, J. B., & Stern, R. J. (2016). The geology of Cuba: A brief overview and synthesis. *GSA Today*, *26*(10). https://doi.org/10.1130/GSATG296A.1

Jackson, M. G., & Macdonald, F. (2022). Hemispheric geochemical dichotomy of the mantle is a legacy of austral supercontinent assembly and onset of deep continental crust subduction. *AGU Advances*, *3*(6), e2022AV000664.

Jutzeler, M., Marsh, R., van Sebille, E., Mittal, T., Carey, R. J., Fauria, K. E., et al. (2020). Ongoing Dispersal of the 7 August 2019 Pumice Raft From the Tonga Arc in the Southwestern Pacific Ocean. *Geophysical Research Letters*, *47*(5), e1701121. https://doi.org/10.1029/2019GL086768

Kaneoka, I., & Katsui, Y. (1985). K-Ar ages of volcanic rocks from Easter Island. *Second Series Bulletin of the Volcanological Society of Japan*, *30*(1), 33–36.

Knesel, K. M., Cohen, B. E., Vasconcelos, P. M., & Thiede, D. S. (2008). Rapid change in drift of the Australian plate records collision with Ontong Java plateau. *Nature*, *454*(7205), 754–757.

Le Roux, P., Le Roex, A., Schilling, J.-G., Shimizu, N., Perkins, W., & Pearce, N. (2002). Mantle heterogeneity beneath the southern Mid-Atlantic Ridge: trace element evidence for contamination of ambient asthenospheric mantle. *Earth and Planetary Science Letters*, *203*(1), 479–498.

Lian, D., Yang, J., Dilek, Y., Wiedenbeck, M., Wu, W., & Rocholl, A. (2020). Precambrian zircons in chromitites of the Cretaceous Aladag ophiolite (Turkey) indicate deep crustal recycling in oceanic mantle. *Precambrian Research*, *350*, 105838.

Lissenberg, C. J., Rioux, M., Shimizu, N., Bowring, S. A., & Mével, C. (2009). Zircon dating of oceanic crustal accretion. *Science*, *323*(5917), 1048–1050.

Liu, C.-Z., Dick, H. J. B., Mitchell, R. N., Wei, W., Zhang, Z.-Y., Hofmann, A. W., et al. (2022). Archean cratonic mantle recycled at a mid-ocean ridge. *Science Advances*, *8*(22), eabn6749. https://doi.org/10.1126/sciadv.abn6749

Miki, M., Inokuchi, H., Yamaguchi, S., Matsuda, J., Nagao, K., Isezaki, N., & Yaskawa, K. (1998). Geomagnetic paleosecular variation in Easter Island, the southeast Pacific. *Physics of the Earth and Planetary Interiors*, *106*(1–2), 93–101.

Moghadam, H. S., Li, Q., Stern, R., Griffin, W., & O'Reilly, S. Y. (2022). Zircon xenocrysts in Late Cretaceous magmatic rocks in the Kermanshah Ophiolite: link to Iran continental crust supports the subduction initiation model. *International Geology Review*, *64*(22), 3248–3259.

Naar, D. F., & Hey, R. N. (1989). Recent Pacific-Easter-Nazca plate motions. *Evolution of Mid Ocean Ridges*, *57*, 9–30.

Ohno, Y., Iguchi, A., Ijima, M., Yasumoto, K., & Suzuki, A. (2022). Coastal ecological impacts from pumice rafts. *Scientific Reports*, *12*(1), 11187. https://doi.org/10.1038/s41598-022-14614-y

Pilot, J., Werner, C.-D., Haubrich, F., & Baumann, N. (1998). Palaeozoic and Proterozoic zircons from the Mid-Atlantic Ridge. *Nature*, *393*(6686), 676–679. https://doi.org/10.1038/31452

Portner, R. A., Murphy, M. J., & Daczko, N. R. (2011). A detrital record of lower oceanic crust exhumation within a Miocene slow-spreading ridge: Macquarie Island, Southern Ocean. *Geological Society of America Bulletin*, *123*(1–2), 255–273. https://doi.org/10.1130/B30082.1

Proenza, J., González-Jiménez, J. M., Garcia-Casco, A., Belousova, E., Griffin, W., Talavera, C., et al. (2018). Cold plumes trigger contamination of oceanic mantle wedges with continental crust-derived sediments: Evidence from chromitite zircon grains of eastern Cuban ophiolites. *Geoscience Frontiers*, *9*(6), 1921–1936.

Rappaport, Y., Naar, D. F., Barton, C. C., Liu, Z. J., & Hey, R. N. (1997). Morphology and distribution of seamounts surrounding Easter Island. *Journal of Geophysical Research: Solid Earth*, *102*(B11), 24713–24728. https://doi.org/10.1029/97JB01634

Ray, J. S., Mahoney, J. J., Duncan, R. A., Ray, J., Wessel, P., & Naar, D. F. (2012). Chronology and Geochemistry of Lavas from the Nazca Ridge and Easter Seamount Chain: an ∼30 Myr Hotspot Record. *Journal of Petrology*, *53*(7), 1417–1448. https://doi.org/10.1093/petrology/egs021

Richter, M., Nebel, O., Maas, R., Mather, B., Nebel-Jacobsen, Y., Capitanio, F. A., et al. (2020). An Early Cretaceous subduction-modified mantle underneath the ultraslow spreading Gakkel Ridge, Arctic Ocean. *Science Advances*, *6*(44). https://doi.org/10.1126/sciadv.abb4340

Rioux, M., Cheadle, M. J., John, B. E., & Bowring, S. A. (2016). The temporal and spatial distribution of magmatism during lower crustal accretion at an ultraslow-spreading ridge: High-precision U–Pb zircon dating of ODP Holes 735B and 1105A, Atlantis Bank, Southwest Indian Ridge. *Earth and Planetary Science Letters*, *449*, 395–406.

Rodrigo, C., DÃ\-az, J., & GonzÃ!`lez-FernÃ!`ndez, A. (2014). Origin of the Easter Submarine Alignment: morphology and structural lineaments. *Latin American Journal of Aquatic Research*, *42*, 857–870.

Rodriguez-Corcho, A. F., Rojas-Agramonte, Y., Barrera-Gonzalez, J. A., Marroquin-Gomez, M. P., Bonilla-Correa, S., Izquierdo-Camacho, D., et al. (2022). The Colombian geochronological database (CGD). *International Geology Review*, *64*(12), 1635–1669.

Rojas-Agramonte, Y., Williams, I. S., Arculus, R., Kröner, A., García-Casco, A., Lázaro, C., et al. (2017). Ancient xenocrystic zircon in young volcanic rocks of the southern Lesser Antilles island arc. *Lithos*, *290–291*. https://doi.org/10.1016/j.lithos.2017.08.002

Rojas-Agramonte, Y., Kaus, B. J., Piccolo, A., Williams, I. S., Gerdes, A., Wong, J., et al. (2022). Zircon Dates Long-Lived Plume Dynamics in Oceanic Islands. *Geochemistry, Geophysics, Geosystems*, *23*(11), e2022GC010485.

Rojas-Agramonte, Yamirka, Garcia-Casco, A., Kemp, A. I. S., Kröner, A., Proenza, J. A., Lázaro, C., & Liu, D. (2016). Recycling and transport of continental material through the mantle wedge above subduction zones: A Caribbean example. *Earth and Planetary Science Letters*, *436*, 93–107.

Rojas-Agramonte, Yamirka, Kaus, B. J. P., Piccolo, A., Williams, I. S., Gerdes, A., Wong, J., et al. (2022). Zircon Dates Long-Lived Plume Dynamics in Oceanic Islands. *Geochemistry, Geophysics, Geosystems*, *23*(11), e2022GC010485. https://doi.org/10.1029/2022GC010485

Rosenbaum, G., Giles, D., Saxon, M., Betts, P. G., Weinberg, R. F., & Duboz, C. (2005). Subduction of the Nazca Ridge and the Inca Plateau: Insights into the formation of ore deposits in Peru. *Earth and Planetary Science Letters*, *239*(1–2), 18–32.

Seelos, K., Rojas-Agramonte, Y., Kröner, A., Toulkeridis, T., Inderwies, G., & Buelow, Y. (2021). Composition and provenance analysis of beach sands in an almost isolated sedimentary system – A field study of the Galápagos Archipelago. *American Journal of Science*, *321*(6), 888. https://doi.org/10.2475/05.2021.04

Sevastjanova, I., Clements, B., Hall, R., Belousova, E. A., Griffin, W. L., & Pearson, N. (2011). Granitic magmatism, basement ages, and provenance indicators in the Malay Peninsula: Insights from detrital zircon U–Pb and Hf-isotope data. *Gondwana Research*, *19*(4), 1024–1039. https://doi.org/10.1016/j.gr.2010.10.010

Simon, N. S. C., Neumann, E.-R., Bonadiman, C., Coltorti, M., Delpech, G., Grégoire, M., & Widom, E. (2008). Ultra-refractory Domains in the Oceanic Mantle Lithosphere Sampled as Mantle Xenoliths at Ocean Islands. *Journal of Petrology*, *49*(6), 1223–1251. https://doi.org/10.1093/petrology/egn023

Simons, K., Dixon, J., Schilling, J.-G., Kingsley, R., & Poreda, R. (2002). Volatiles in basaltic glasses from the Easter-Salas y Gomez Seamount Chain and Easter Microplate: Implications for geochemical cycling of volatile elements. *Geochemistry, Geophysics, Geosystems*, *3*(7), 1–29. https://doi.org/10.1029/2001GC000173

Skublov, S. G., Rumyantseva, N. A., Li, Q., Vanshtein, B. G., Rezvukhin, D. I., & Li, X. (2022). Zircon Xenocrysts from the Shaka Ridge Record Ancient Continental Crust: New U-Pb Geochronological and Oxygen Isotopic Data. *Journal of Earth Science*, *33*(1), 5–16. https://doi.org/10.1007/s12583-021-1422-2

Stoffers, P., Hékinian, R., & Haase, K. M. (1994). Geology of young submarine volcanoes west of Easter Island, Southeast Pacific. *Marine Geology*, *118*(3), 177–185. https://doi.org/10.1016/0025-3227(94)90081-7

Torsvik, T. H., & Cocks, L. R. M. (2019). The integration of palaeomagnetism, the geological record and mantle tomography in the location of ancient continents. *Geological Magazine*, *156*(2), 242–260.

Torsvik, T. H., Amundsen, H., Hartz, E. H., Corfu, F., Kusznir, N., Gaina, C., et al. (2013). A Precambrian microcontinent in the Indian Ocean. *Nature Geoscience*, *6*(3), 223–227. https://doi.org/10.1038/ngeo1736

Torsvik, T. H., Steinberger, B., Shephard, G. E., Doubrovine, P. V., Gaina, C., Domeier, M., et al. (2019). Pacific-Panthalassic reconstructions: Overview, errata and the way forward. *Geochemistry, Geophysics, Geosystems*, *20*(7), 3659–3689.

Urann, B., Dick, H., Parnell-Turner, R., & Casey, J. (2020). Recycled arc mantle recovered from the Mid-Atlantic Ridge. *Nature Communications*, *11*(1), 3887.

Valley, J. W. (2003). Oxygen Isotopes in Zircon. *Reviews in Mineralogy and Geochemistry*, *53*(1), 343–385. https://doi.org/10.2113/0530343

van de Lagemaat, S. H., Cao, L., Asis, J., Advokaat, E., Mason, P., Dekkers, M. J., & van Hinsbergen, D. J. (2023). Causes of Late Cretaceous subduction termination below South China and Borneo: Was the Proto-South China Sea underlain by an oceanic plateau?

Van der Meer, D. G., Van Hinsbergen, D. J., & Spakman, W. (2018). Atlas of the underworld: Slab remnants in the mantle, their sinking history, and a new outlook on lower mantle viscosity. *Tectonophysics*, *723*, 309–448.

van Hinsbergen, D. J., Spakman, W., de Boorder, H., Van Dongen, M., Jowitt, S. M., & Mason, P. R. (2020). Arc-type magmatism due to continental-edge plowing through ancient subduction-enriched mantle. *Geophysical Research Letters*, *47*(9), e2020GL087484.

Van Hinsbergen, D. J., & Schouten, T. L. (2021). Deciphering paleogeography from orogenic architecture: constructing orogens in a future supercontinent as thought experiment. *American Journal of Science*, *321*(6), 955–1031.

Vaughan, A. P., Kelley, S. P., & Storey, B. C. (2002). Mid-Cretaceous ductile deformation on the Eastern Palmer Land Shear Zone, Antarctica, and implications for timing of Mesozoic terrane collision. *Geological Magazine*, *139*(4), 465–471.

Vaughan, A. P., Eagles, G., & Flowerdew, M. J. (2012). Evidence for a two-phase Palmer Land event from crosscutting structural relationships and emplacement timing of the Lassiter Coast Intrusive Suite, Antarctic Peninsula: Implications for mid-Cretaceous Southern Ocean plate configuration. *Tectonics*, *31*(1).

Vezzoli, L., & Acocella, V. (2009). Easter Island, SE Pacific: An end-member type of hotspot volcanism. *GSA Bulletin*, *121*(5–6), 869–886. https://doi.org/10.1130/B26470.1

Wu, Y., Fang, X., & Ji, J. (2023). A global zircon U–Th–Pb geochronology database. *Earth System Science Data Discussions*, *2023*, 1–20. https://doi.org/10.5194/essd-2023-20

Xiong, F., Zoheir, B., Xu, X., Lenaz, D., & Yang, J. (2022). Genesis and high-pressure evolution of the Köyceğiz ophiolite (SW Turkey): Mineralogical and geochemical characteristics of podiform chromitites. *Ore Geology Reviews*, *145*, 104912.

Yang, F., Kim, S. W., Tsunogae, T., & Zhou, H. (2021). Multiple enrichment of subcontinental lithospheric mantle with Archean to Mesozoic components: Evidence from the Chicheng ultramafic complex, North China Craton. *Gondwana Research*, *94*, 201–221.